



Landslide susceptibility zonation of the Western Ghats region in Thiruvananthapuram district (Kerala) using geospatial tools: A comparison of the AHP and Fuzzy-AHP methods

M. Akshaya¹ · Jean Homian Danumah² · Sunil Saha³ · R. S. Ajin⁴ · Sekhar L. Kuriakose⁴

Received: 1 June 2021 / Revised: 7 September 2021 / Accepted: 8 September 2021 / Published online: 6 October 2021
© The Author(s), under exclusive licence to Springer Nature Switzerland AG 2021

Abstract

Landslides are one of the most common geohazards occurring in the Western Ghats region of Kerala, causing substantial loss of life and property. The present study aims to demarcate the landslide susceptible zones in the Western Ghats region of Thiruvananthapuram district using GIS techniques. The analytical hierarchy process (AHP) and fuzzy-analytical hierarchy process (F-AHP) methods are used to derive the weights. Eleven causative factors, viz. slope angle, elevation, aspect, road buffer, land use/land cover types, sediment transport index, stream power index, drainage buffer, lithology, soil texture, and lineament buffer have been considered for the mapping process. The area of the susceptibility maps was categorized into five zones: very low, low, moderate, high, and very high. This study confirmed that the majority of landslides occurred due to anthropogenic reasons (road cuttings). Finally, the receiver operating characteristic (ROC) curve method was used to validate the landslide susceptibility maps. The area under the ROC curve (AUC) value was above 0.70 for both the AHP (0.71) and F-AHP (0.76) methods. Hence, it is confirmed that the F-AHP model is more effective in demarcating landslide susceptible zones. As per the landslide susceptibility map created using the F-AHP model, 10.97% of the study area is categorized as very high susceptible. The result of the study will help policy makers and planners to implement effective mitigation measures to prevent landslides along the road cuttings in other areas with similar geomorphological characteristics.

Keywords AHP · Landslides · Road cuttings · ROC curve · Western Ghats

Introduction

Landslides, the most common type of geohazard in mountainous terrain, are caused by both intrinsic and extrinsic factors (Bachri et al. 2021). The intrinsic (internal) factors include bedrock geology, geomorphology, soil depth, soil type, slope gradient, slope aspect, slope curvature,

elevation, land use pattern, drainage pattern, etc. (Dahal et al. 2012), whereas the extrinsic/external (triggering) factors are rainfall, seismicity, and anthropogenic activities (Getachew and Meten 2021). The intrinsic factors represent the inherent characteristics of the ground that make the slopes susceptible to landslides (Getachew and Meten 2021). Landslides can result in loss of human life, property damage, and economic crisis (Youssef and Pourghasemi 2021). It can adversely affect the topography, character and quality of rivers and streams, and groundwater flow, forests, and wildlife habitat (Geertsema et al. 2009). According to the NDMA (2019), the Western Ghats region in states such as Maharashtra, Karnataka, Goa, and Kerala are vulnerable to landslides. This region is characterized by rugged hills with steep slopes, wherein loose soil and earth materials lie above Precambrian crystalline rocks (Sajinkumar et al. 2011). In this region, activities such as deforestation, obstructing ephemeral streams, and the cultivation of crops deficient in the ability to provide root cohesiveness to steep slopes have been speeding up the

✉ R. S. Ajin
ajinares@gmail.com; ajinares@ieee.org

¹ Department of Geology, University College, Thiruvananthapuram, Kerala, India

² Centre Universitaire de Recherche et d'Application en Télédétection (CURAT), Université Félix Houphouët-Boigny, Abidjan, Côte d'Ivoire

³ Department of Geography, University of Gour Banga, Malda, West Bengal, India

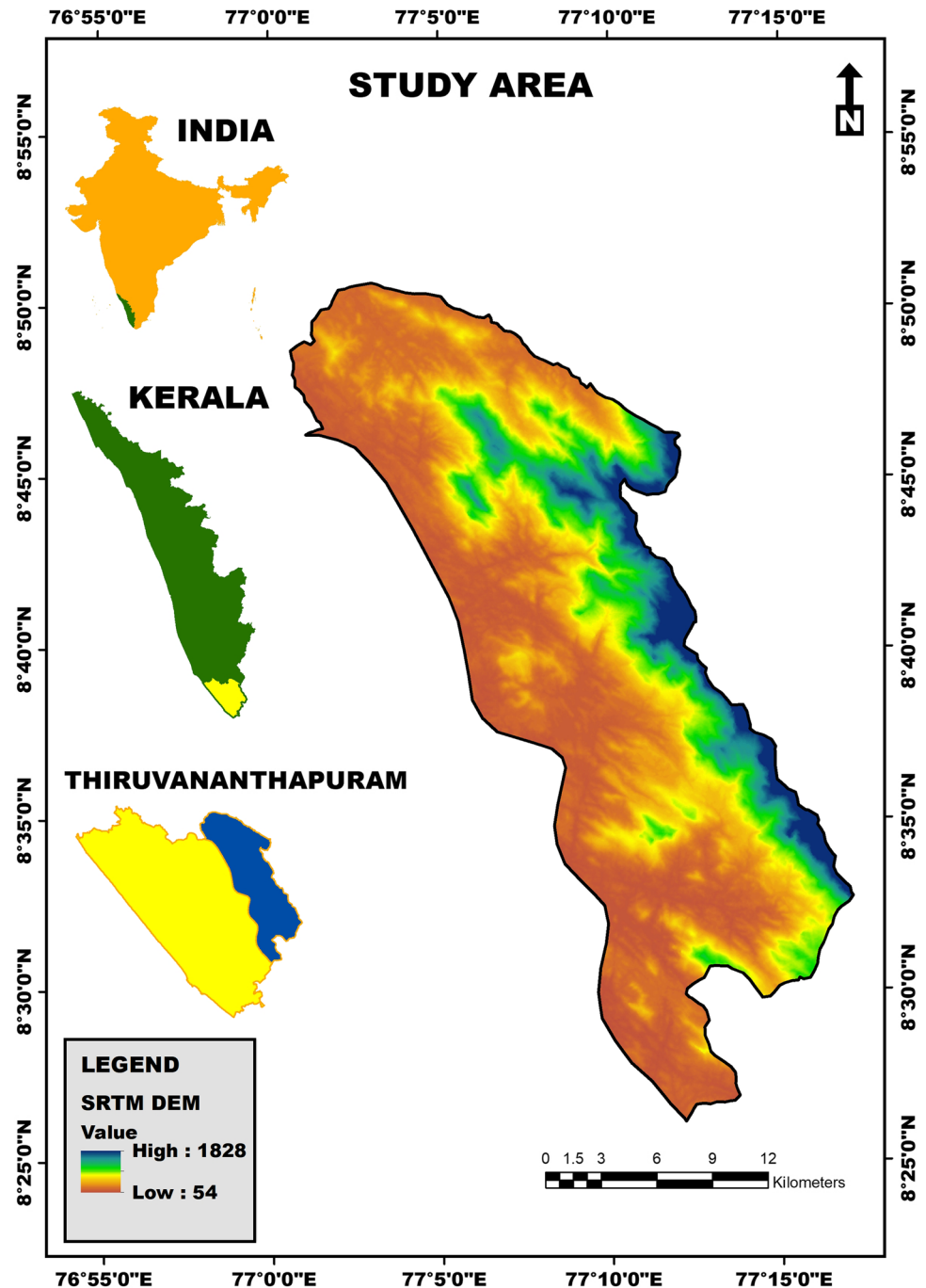
⁴ Kerala State Emergency Operations Centre (KSEOC), Kerala State Disaster Management Authority (KSDMA), Thiruvananthapuram, India

processes leading to landslides (Kuriakose et al. 2009). Hence, the demarcation of landslide susceptible zones in this region will help in preventing or reducing the adverse effects and loss of life and property due to landslides.

Many researchers used geospatial tools to delineate the landslide susceptible zones in the Western Ghats region of Kerala (Prasannakumar and Vijith 2012; Vijith et al. 2014; Feby et al. 2020). The various methods used in landslide susceptibility zonation include AHP (Hasekiogulları and Ercanoglu 2012; Kayastha et al. 2013b; El Jazouli et al.

2019; Basu and Pal 2020), frequency ratio (Vijith and Madhu 2007; Jana et al. 2019; Pal and Chowdhuri 2019; Zhang et al. 2020; Shano et al. 2021), fuzzy logic (Kayastha 2012; Kayastha et al. 2013a; Rostami et al. 2016; Fatemi Aghda et al. 2018), F-AHP (Mokarram and Zarei 2018; Sur et al. 2020; Zhou et al. 2020), artificial neural network (Lee et al. 2006; Tsangaratos and Benardos 2014; Harmouzi et al. 2019; Zeng and Chen 2021), analytical network process (Sujatha and Sridhar 2017; Sujatha 2020; Swetha and Gopinath 2020), logistic regression (Chauhan et al.

Fig. 1 The study area



2010; Ramani et al. 2011; Talaei 2014; Mandal and Mandal 2018), index of entropy (Constantin et al. 2011; Mondal and Mandal 2019), support vector machine (Pourghasemi et al. 2013; Du et al. 2016; Wu et al. 2016; Lee et al. 2017), random forest (Taalab et al. 2018; Rahmati et al. 2021), etc. Researchers like Demir et al. (2013), Pham et al. (2016), Aditian et al. (2018), Nhu et al. (2020), Ali et al. (2021), and Youssef and Pourghasemi (2021) used two or more different methods to compare the efficacy of those methods in landslide susceptibility zonation. In previous studies, different statistical and machine learning methods have been used. In this research, we used a semi-quantitative method (AHP) and an ensemble of AHP and Fuzzy logic methods (Fuzzy-AHP), which are still not applied in the present study area. AHP simplifies complex problems into multiple simple, hierarchically linked problems, and the factors are ranked after the hierarchical formation utilizing pair comparisons (Gompf et al. 2021). The paired comparison helps the decision-maker to prioritize only two options under comparison, regardless of other options (Gompf et al. 2021). The Fuzzy logic theory was integrated

into the AHP method to develop the Fuzzy-AHP method (Putra et al. 2018). AHP method's inability to address the imprecision and subjectivity in the judgements will be rectified by utilizing fuzzy AHP (Carnero 2017).

The objectives of this study are to demarcate the landslide susceptible zone of the Western Ghats region in Thiruvananthapuram district using AHP and F-AHP methods, to assess the influence of each causative factor on the initiation of landslides, to compare the efficacy of both AHP and F-AHP methods, and to ascertain whether the integration of Fuzzy logic and AHP methods provide better result than the AHP method.

Materials and methods

Study area

The study area lies between latitudes of 8°25'–8°55' N and longitudes of 77°0'–77°20' E. This area spans an area of 524.38 km² in the southern Western Ghats (Fig. 1). This

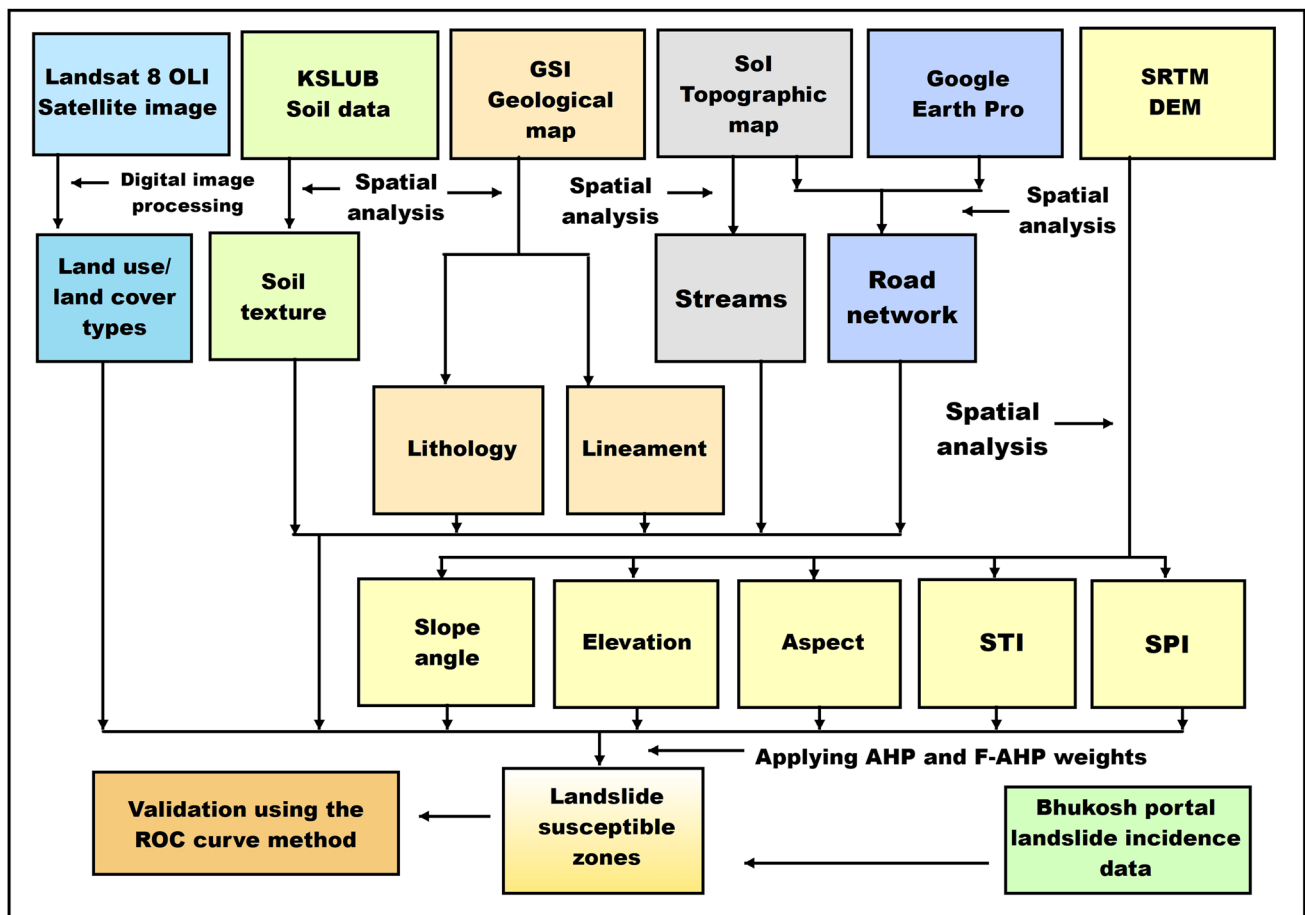


Fig. 2 Flowchart of the landslide susceptibility modelling

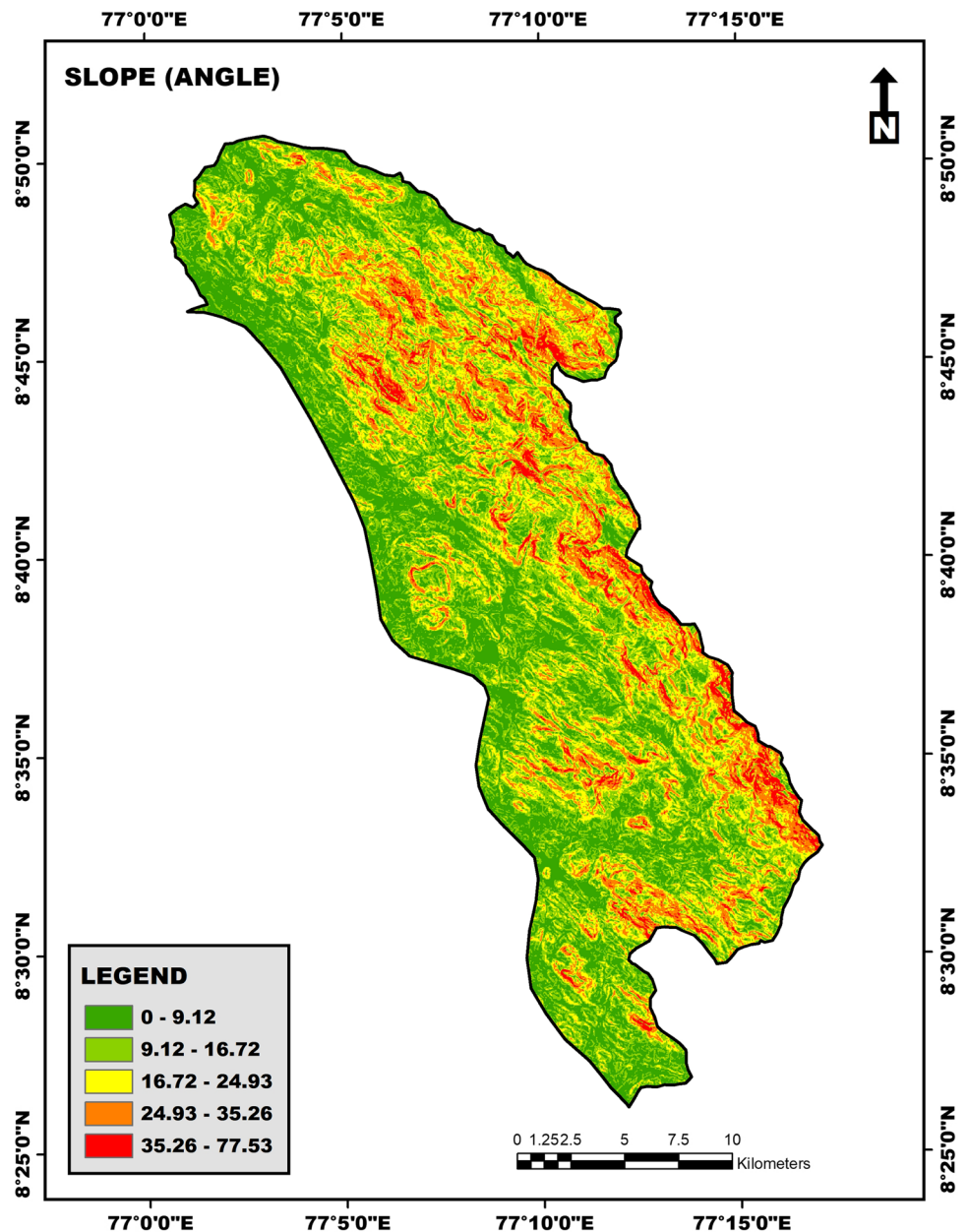
portion of the Western Ghats has been affected by landslides in the past, and a devastating landslide occurred in Amboori on 9 November 2001, resulting in the death of 38 people (Naidu et al. 2018).

Data used

The study area lies on the Survey of India (SoI) topographic maps numbered 58 H/1, 58 H/2, 58 H/3, and 58 H/6 at 1:50,000 scale. The data used for this study includes the Landsat 8 OLI satellite images, the Shuttle Radar Topography Mission (SRTM) digital elevation model (DEM), the geological map prepared by the Geological Survey of India (GSI), soil data collected from the Kerala State Land Use

Board (KSLUB), SoI topographic maps, and Google Earth Pro data. The ArcGIS 10.8 and ERDAS Imagine 8.4 software tools have been used to create the thematic layers of factors such as slope angle, elevation, aspect, road buffer, land use/land cover (LULC), sediment transport index (STI), stream power index (SPI), stream buffer, lithology, soil texture, and lineament buffer. The thematic layers of factors such as slope, elevation, STI, and SPI were classified using the natural breaks (Jenks) classification method included with the ArcGIS software. All thematic layers were resampled to a spatial resolution of 30 m. After assigning the weights determined by the AHP and F-AHP methods, the thematic layers of the selected factors were combined using the raster calculator tool in the ArcGIS software to generate landslide-susceptible

Fig. 3 Slope



zone maps. The landslide incidence data from the Bhukosh portal (<https://bhukosh.gsi.gov.in/>) of the GSI was used to validate the prepared landslide susceptible zone maps. The RStudio software has been used for ROC curve analysis and to estimate the AUC values. The flowchart of the landslide susceptibility modelling is depicted in Fig. 2.

Causative factors

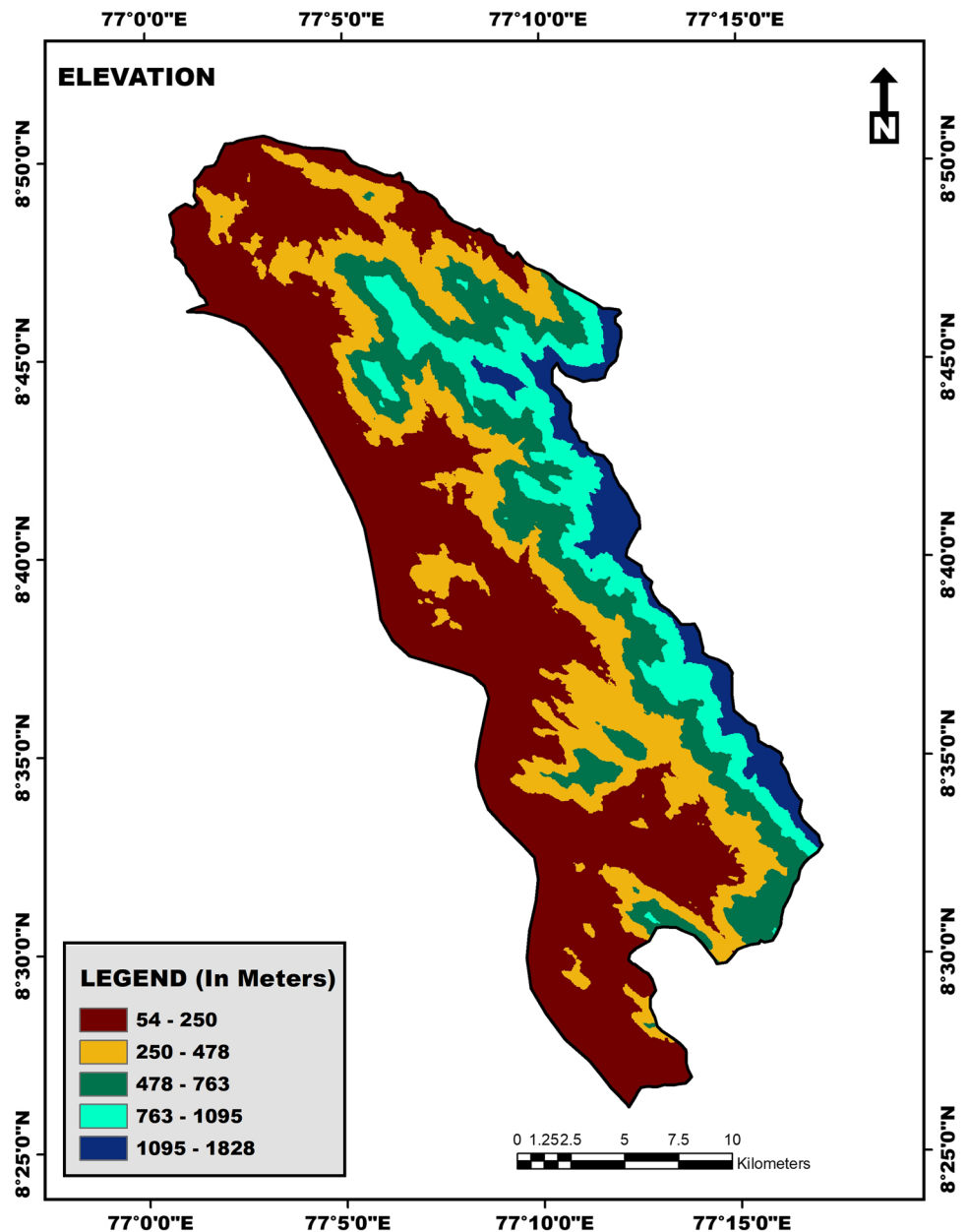
Slope angle The chance of landslides increases with an increase in slope angle (Nachappa et al. 2020; Youssef and Pourghasemi 2021). The slope was derived from the SRTM

DEM at 30 m spatial resolution using ArcGIS spatial analyst tools. The slope of this area ranges between 0° and 77.53° and is grouped into five classes (Fig. 3).

Elevation The SRTM DEM was used to derive the elevation of the study area. The elevation of the study area ranges from 54 to 1828 (Fig. 4) and is grouped into 5 classes. A study by Nakileza and Nedala (2020) found that the number of landslides will be high in areas with an elevation ranging from 1500 to 1800 m.

Aspect The aspect determines the slope’s exposure to sunlight and prevailing winds, and this influences the soil moisture on the slopes (Xiao et al. 2019). In the northern

Fig. 4 Elevation



hemisphere, south-facing and west-facing slopes are exposed to intense solar radiation (Setiawan et al. 2004). The aspect was also derived from the SRTM DEM using ArcGIS spatial analyst tools. The slope aspect of this area is categorized into nine classes: Flat, North, Northeast, East, Southeast, South, Southwest, West, Northwest (Fig. 5).

Road buffer The road is one of the most important anthropogenic factors influencing the occurrence of landslides (Nachappa et al. 2020). Construction of roads along hills or mountains can increase the instability of slopes (Wang et al. 2016) by introducing seepage conditions that may lead to further breakdown of the slope (Aditian et al.

2018). Engineering activities like cutting and excavating of slopes can weaken the natural support of slopes (Youssef and Pourghasemi 2021). The road networks were digitized from the SoI topographic maps and Google Earth Pro. The proximity tool in ArcGIS software was used to create the 100 m buffer road data and is depicted in Fig. 6.

Land use/land cover types Land cover reduces the possibility of soil erosion and landslides (Reis et al. 2012), whereas land use and landscape changes in hilly areas decrease slope stability and thus promote sliding (Feby et al. 2020). The Landsat 8 OLI satellite image was used to extract land use and land cover types. The maximum

Fig. 5 Aspect

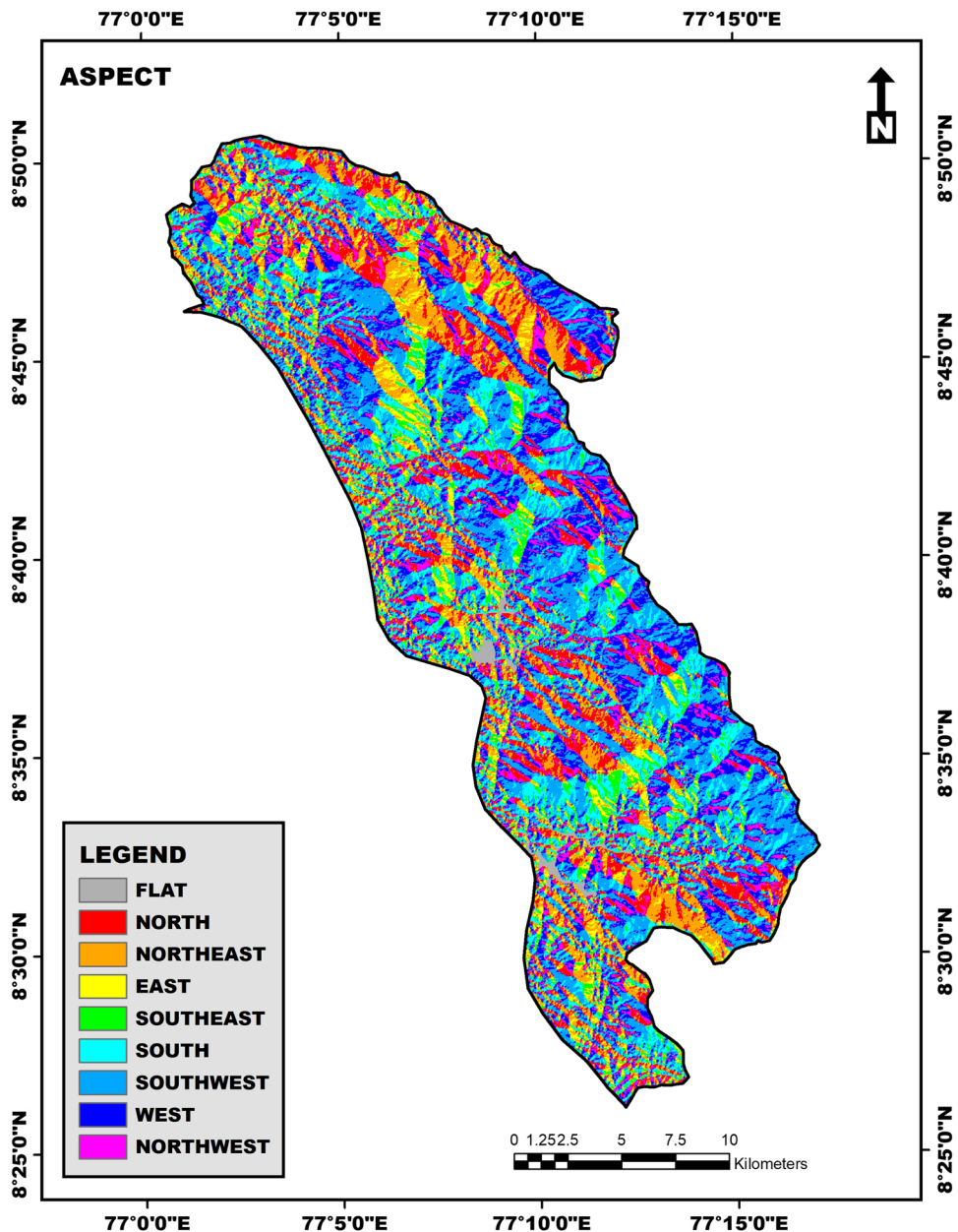
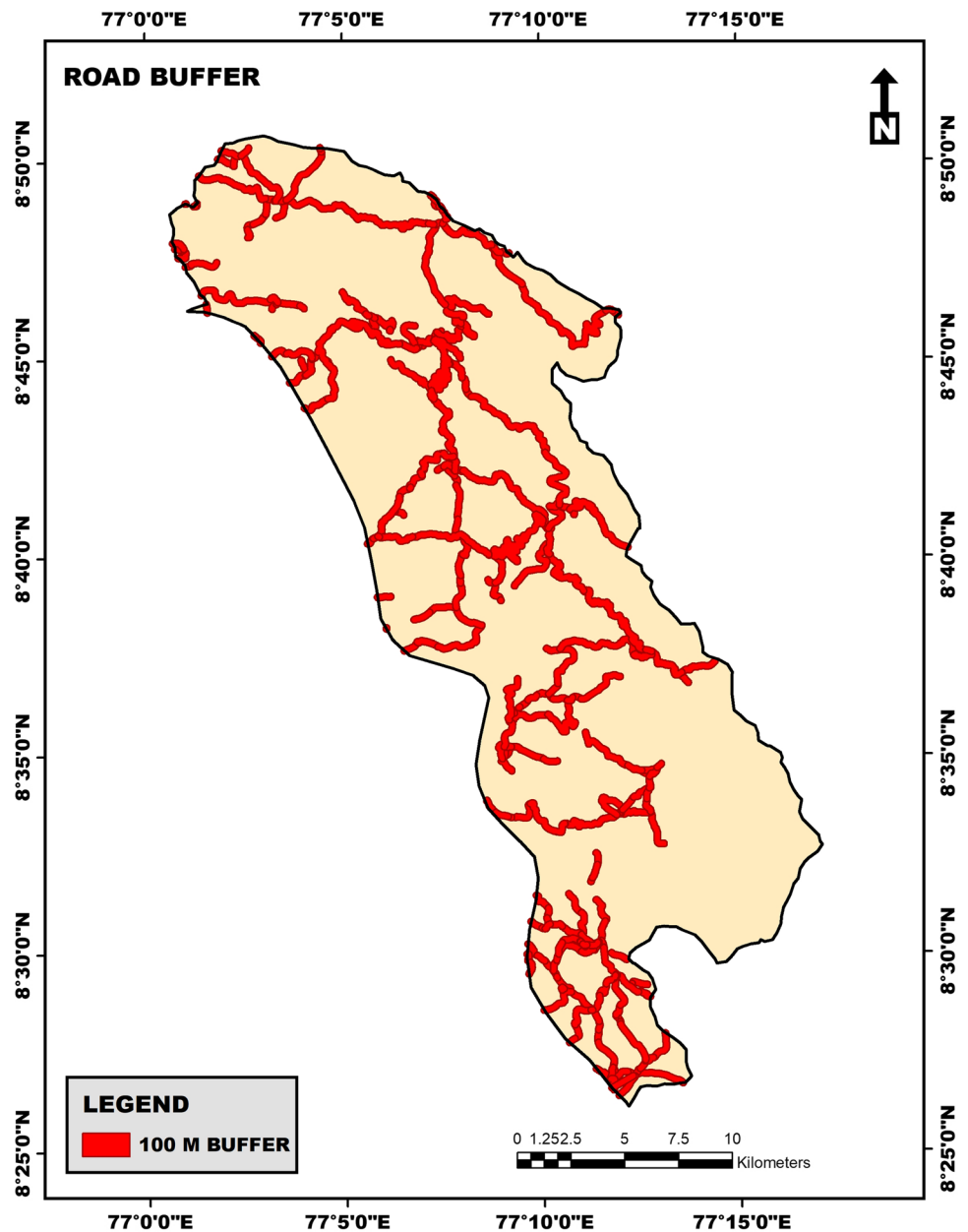


Fig. 6 Road buffer



likelihood classification approach available with the ERDAS Imagine software was used for classifying the various land use/land cover types present in this area. The land use/land cover types present in the study area include agricultural land, built-up areas, barren land, scrubland, deciduous forest, evergreen forest, and water bodies (Fig. 7).

Sediment transport index STI reflects the erosive power of the overland flow (Pourghasemi et al. 2012). STI was derived from the SRTM DEM using ArcGIS spatial analyst tools and Eq. 1 (Moore et al. 1993).

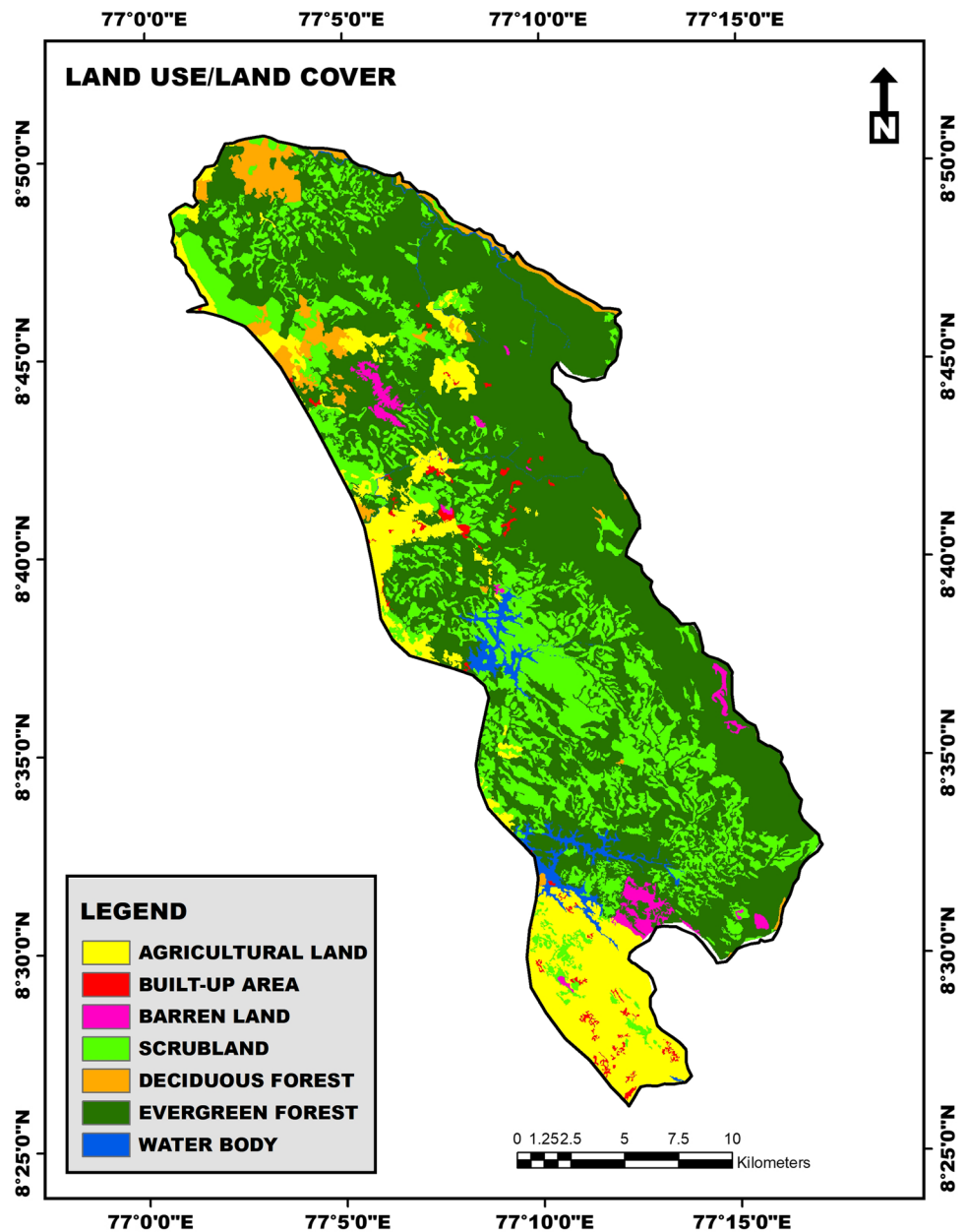
$$STI = \left(\frac{\alpha}{22.13} \right)^{0.6} \left(\frac{\sin\beta}{0.0896} \right)^{1.3} \tag{1}$$

where α is the area of the catchment (m^2) and β (radians) is the slope gradient.

The STI of this area ranges from 0 to 322.47 (Fig. 8) and is grouped into 5 classes (0–2.52, 2.52–13.91, 13.91–36.67, 36.67–87.25, and 87.25–322.47). The chance of landslides is high in areas with higher STI.

Stream power index The stream power index (SPI) is a measure of the erosive capacity of flowing water (Nhu et al. 2020). The chance of sliding is greater in areas with higher

Fig. 7 Land use/land cover types



SPI. The SPI was derived from the SRTM DEM using ArcGIS spatial analyst tools and Eq. 2 (Moore et al. 1991).

$$SPI = \alpha \tan \beta \quad (2)$$

where α is the specific catchment area and β is the local slope.

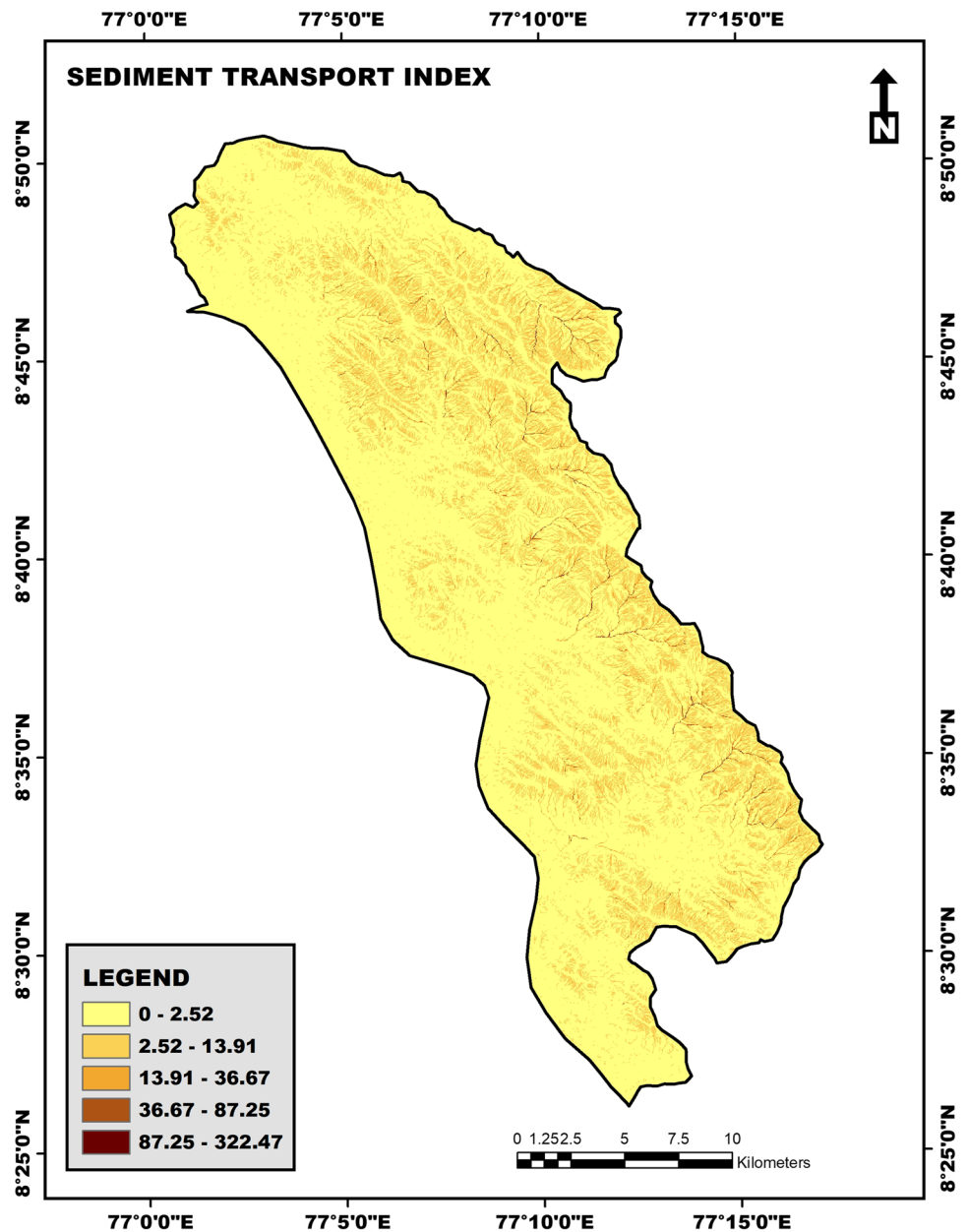
The SPI of the study area ranges from 0 to 9.23 and is grouped into five classes as depicted in Fig. 9.

Stream buffer Streams may adversely affect stability by eroding or by saturating the lower parts of the slopes (Bagherzadeh and Daneshvar 2013). The stream networks were

extracted from the SoI topographic maps, and the stream buffer layer was created using the ArcGIS proximity tool. The 100 m buffer streams of the study area are shown in Fig. 10.

Lithology The strength and permeability of rocks may vary depending on the type of lithological units, and sliding usually occurs along a rock type with lower strength and permeability (Nachappa et al. 2020). In comparison to the weaker rocks, the stronger rocks give more resistance to the driving forces (Bagherzadeh and Daneshvar 2013). The rock types were digitized from the geological map of GSI (at 1:50,000 scale) using ArcGIS tools. The rock types

Fig. 8 Sediment transport index



present in the study area include: charnockite, garnetiferous biotite, and garnet-biotite gneiss (Fig. 11).

Soil texture Soils with a high proportion of clay content are resistant to detachment (Sharma et al. 2012). Also, the rate of soil erosion will be very high in areas with sandy soils (Sharma et al. 2012). The soil data (shape file) at 1:250,000 was collected from the KSLUB. The soil types present in the study area are clay, gravelly clay, gravelly loam, and loam (Fig. 12). The chance of sliding is higher in areas with loam and gravelly loam.

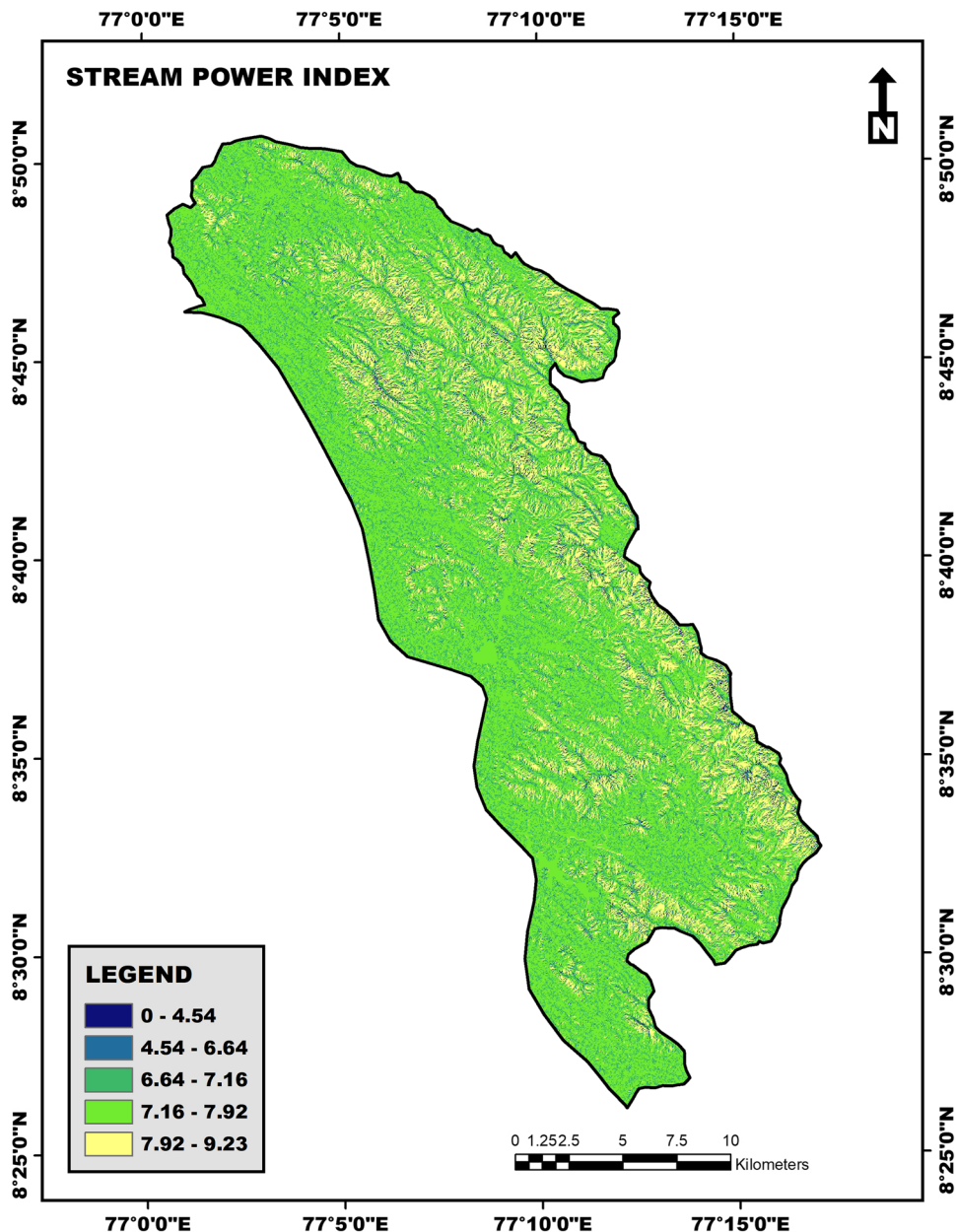
Lineament buffer Lineaments, the mapable linear geological features such as joints, shear zones, faults, and fold axis (Ram et al. 2020), act as potential weak planes which could reduce bulk-rock strength and further

facilitate the process of slope failure (Wu et al. 2020). The lineaments were digitized from the GSI geological map, and the lineament buffer layer was derived using the ArcGIS proximity tool. Figure 13 depicts the 100 m buffer lineaments of this area.

AHP modelling

AHP is a multi-criteria decision-making technique developed by Thomas Saaty (Saaty 1980). This method works on the principal of deconstructing complex issues into a hierarchy and finding a solution that best fits the objective (Qazi and Abushammala 2020). The major steps include construction of a matrix for pair-wise comparison,

Fig. 9 Stream power index



calculation of the eigen vector and weighting coefficient (Table 1), and consistency ratio (Table 2).

where Slp. is the slope angle, Ele. is the elevation, Asp. is the aspect, RB is the road buffer, LULC is the land use/land cover types, STI is the sediment transport index, SPI is the stream power index, SB is the stream buffer, Litho. is the lithology, and LB is the lineament buffer.

The eigen vector (V_p), and weighting coefficient (C_p) were calculated using Eqs. 3 and 4 as follows:

$$V_p = \sqrt[k]{W_1 \times \dots \times W_k} \tag{3}$$

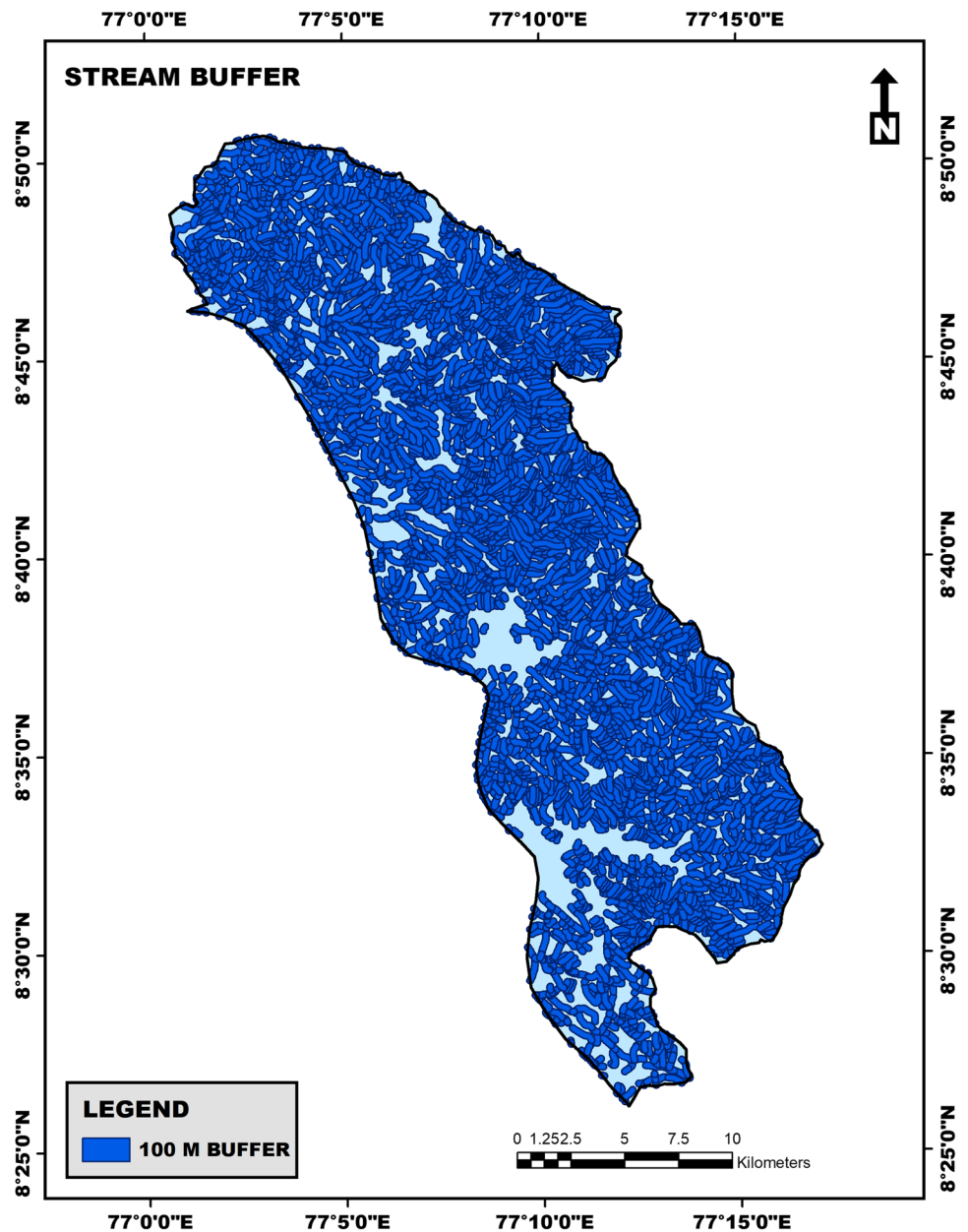
where k is the number of factors, and W is the ratings of the factors.

$$C_p = \frac{V_p}{V_{p1} + \dots + V_{pk}} \tag{4}$$

The matrix was normalized by dividing each element by the sum of the columns. By averaging each row, the priority vector [C] was calculated. The overall priority [D] was computed by multiplying each column of the matrix by the respective priority vector. The rational priority [E] was calculated by dividing each overall priority by the priority.

The eigen value (λ_{max}), consistency index (CI), and consistency ratio (CR) were computed using Eqs. 5, 6, and 7 as follows:

Fig. 10 Stream buffer



$$\lambda_{\max} = \frac{[E]}{k} \tag{5}$$

$$CI = (\lambda_{\max} - k) / (k - 1) \tag{6}$$

$$CR = \frac{CI}{RI} \tag{7}$$

where RI is the random index (Table 3).

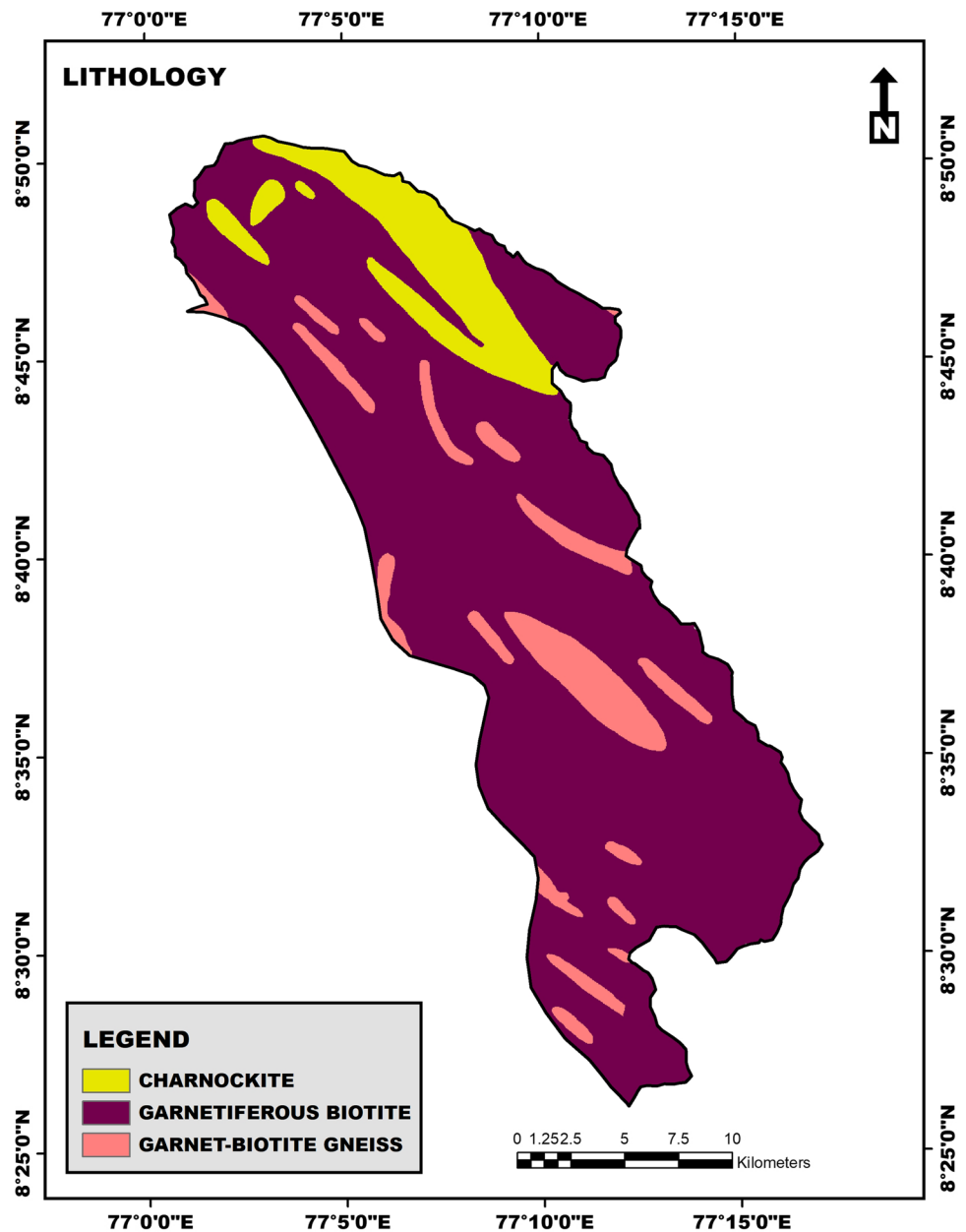
According to Saaty (1980), CR of less than 0.1 is acceptable. If the CR is above 0.1, the exercises should be repeated

until a CR of acceptable consistency is achieved. In this AHP modeling, a CR of acceptable consistency (0.047) was achieved. Hence, the judgments are consistent.

The final weights obtained using the AHP method is shown in Eq. 8.

$$\begin{aligned} LSZ = & (0.276 \times Slp.) + (0.209 \times Ele.) + (0.153 \times Asp.) \\ & + (0.111 \times RB) + (0.079 \times LULC) + (0.056 \times STI) \\ & + (0.040 \times SPI) + (0.029 \times SB) + (0.021 \times Litho.) \\ & + (0.015 \times Soil) + (0.011 \times LB) \end{aligned} \tag{8}$$

Fig. 11 Lithology



Fuzzy-AHP modelling

In this model, a combination of AHP and fuzzy sets is used to weight the effective contributing factors (Eskandari and Miesel 2017). The F-AHP model can be used as a decision-making analysis tool since it handles uncertain and imprecise data (Perçin 2008). The present study adopted the approach of Buckley (1985), which compared fuzzy ratios described by triangular membership functions. The major processes involved are construction of pair-wise comparison (Table 4), calculation of the geometric mean of fuzzy comparison values (Table 5), calculation

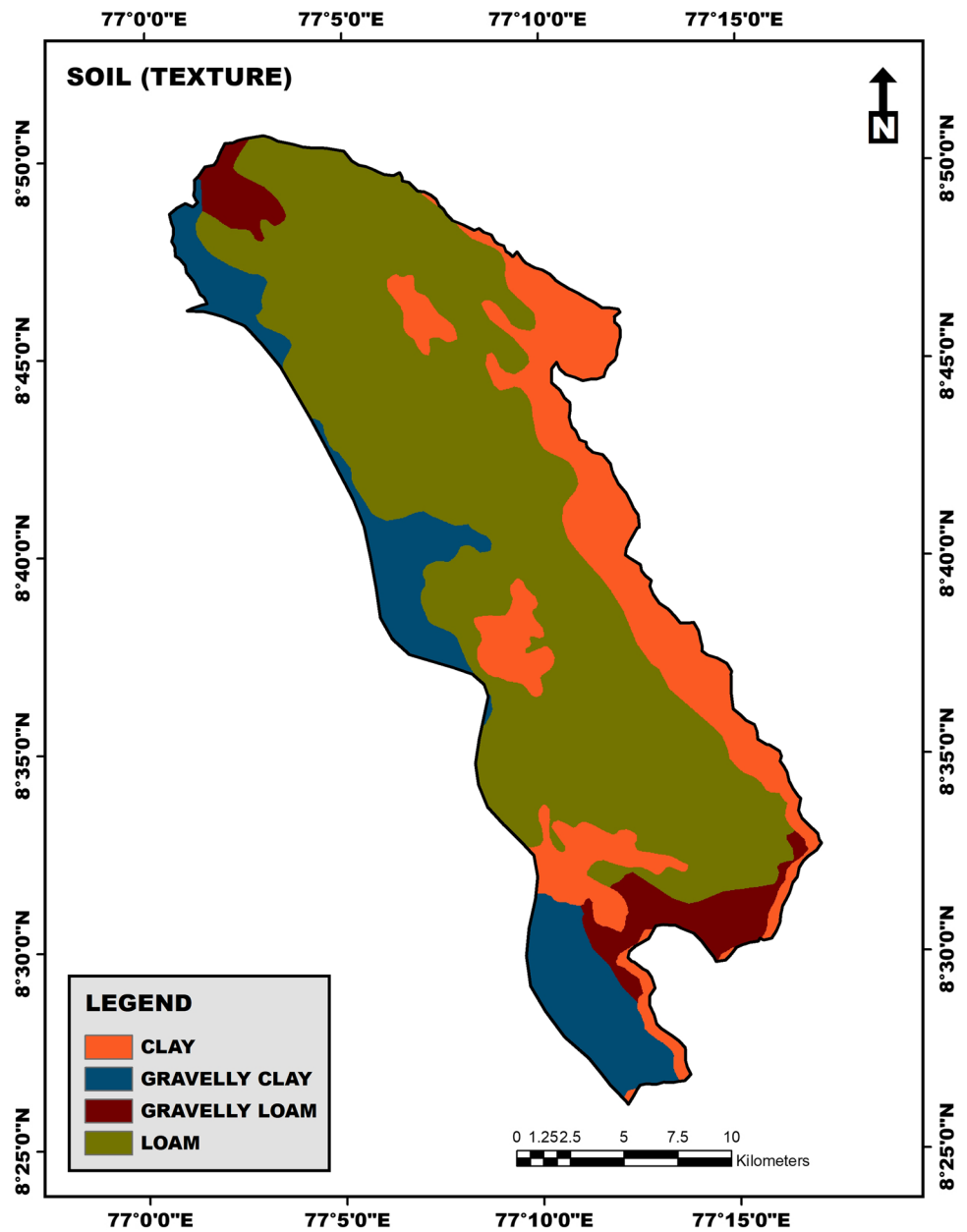
of relative fuzzy weights of each parameter (Table 6), and calculation of averaged and normalized relative weights (Table 7). The various steps involved are as follows:

Step 1: Comparison of the criteria or alternatives by decision makers

For example: When the decision maker states that parameter 1 (P1) is weakly significant than parameter 2 (P2), then the fuzzy triangular scale will be (2, 3, 4). For the pair wise contribution matrix, the fuzzy triangular scale will be (1/4, 1/3, 1/2) (Ayhan 2013).

The pair-wise contribution matrix is demonstrated in Eq. 9.

Fig. 12 Soil texture



$$\tilde{A}^k = \begin{bmatrix} \tilde{d}_{11}^k & \tilde{d}_{12}^k & \dots & \tilde{d}_{1n}^k \\ \tilde{d}_{21}^k & \dots & \dots & \tilde{d}_{2n}^k \\ \dots & \dots & \dots & \dots \\ \tilde{d}_{n1}^k & \tilde{d}_{n2}^k & \dots & \tilde{d}_{nn}^k \end{bmatrix} \tag{9}$$

where \tilde{d}_{ij}^k indicates the kth decision maker’s preference of ith parameter over jth parameter, by the way of fuzzy triangular numbers (Ayhan 2013).

Step 2: The preferences (\tilde{d}_{ij}^k) were averaged, and (\tilde{d}_{ij}) was calculated using Eq. 10.

$$\tilde{d}_{ij} = \frac{\sum_{k=1}^K \tilde{d}_{ij}^k}{K} \tag{10}$$

Step 3: Modification of the pair-wise comparison matrix based on the averaged preferences using Eq. 11.

$$\tilde{A} = \begin{bmatrix} \tilde{d}_{11} & \dots & \tilde{d}_{1n} \\ \vdots & \ddots & \vdots \\ \tilde{d}_{n1} & \dots & \tilde{d}_{nn} \end{bmatrix} \tag{11}$$

Step 4: Calculation of the geometric average of fuzzy comparative values for each parameter using Eq. 12 (Buckley 1985).

$$\tilde{r}_i = \left(\prod_{j=1}^n \tilde{d}_{ij} \right)^{1/n}, i = 1, 2, \dots, n \tag{12}$$

Fig. 13 Lineament buffer

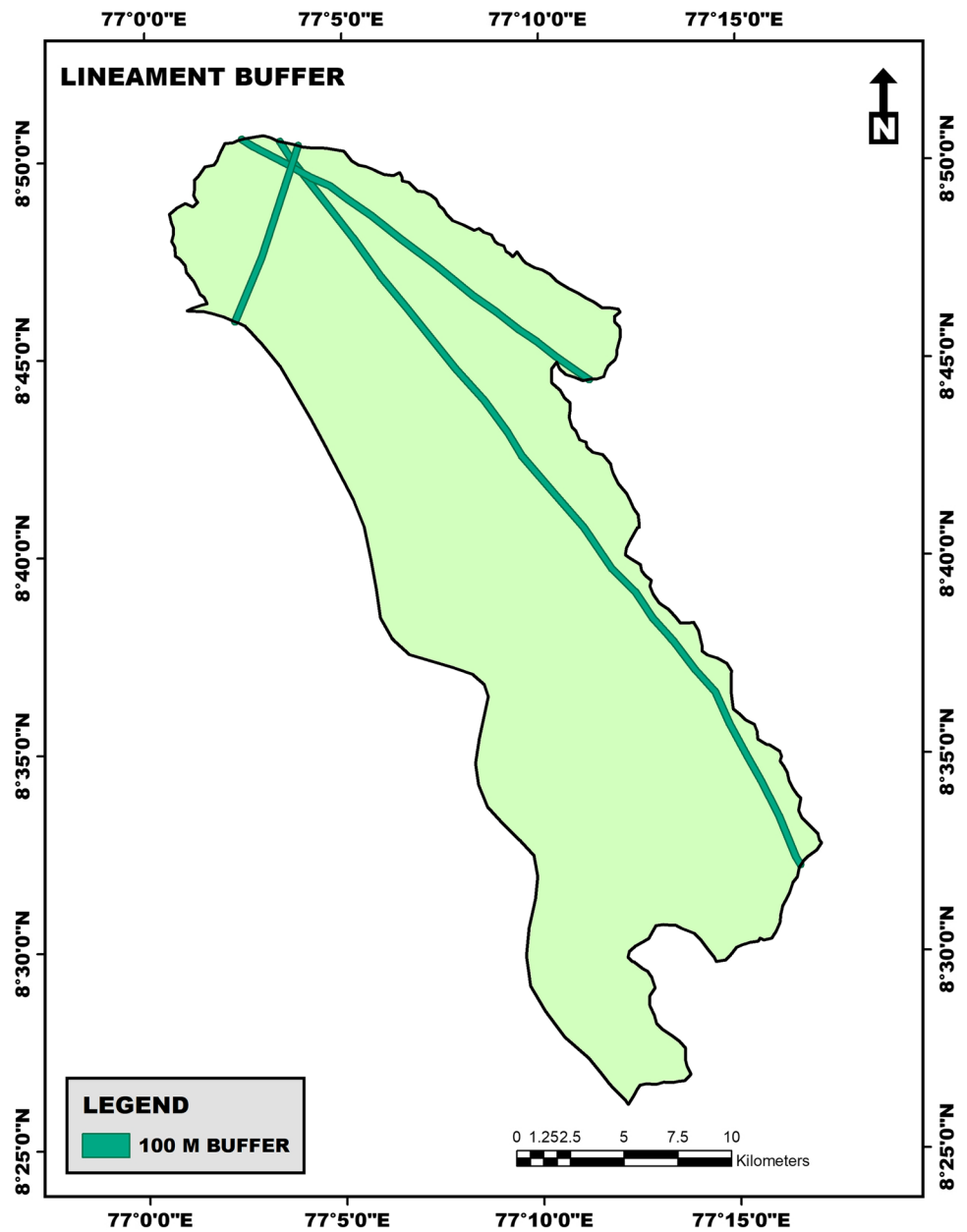


Table 1 Pairwise comparison matrix

	Slp	Ele	Asp.	RB	LULC	STI	SPI	SB	Litho	Soil	LB	Vp	Cp
Slp	1	2	3	4	5	6	7	8	9	10	11	4.909	0.276
Ele	1/2	1	2	3	4	5	6	7	8	9	10	3.707	0.209
Asp.	1/3	1/2	1	2	3	4	5	6	7	8	9	2.721	0.153
RB	1/4	1/3	1/2	1	2	3	4	5	6	7	8	1.964	0.111
LULC	1/5	1/4	1/3	1/2	1	2	3	4	5	6	7	1.405	0.079
STI	1/6	1/5	1/4	1/3	1/2	1	2	3	4	5	6	1.000	0.056
SPI	1/7	1/6	1/5	1/4	1/3	1/2	1	2	3	4	5	0.712	0.040
SB	1/8	1/7	1/6	1/5	1/4	1/3	1/2	1	2	3	4	0.509	0.029
Litho	1/9	1/8	1/7	1/6	1/5	1/4	1/3	1/2	1	2	3	0.368	0.021
Soil	1/10	1/9	1/8	1/7	1/6	1/5	1/4	1/3	1/2	1	2	0.270	0.015
LB	1/11	1/10	1/9	1/8	1/7	1/6	1/5	1/4	1/3	1/2	1	0.204	0.011
Σ	3.02	4.93	7.83	11.72	16.59	22.45	29.28	37.08	45.83	55.50	66.00	17.77	1.00

Table 2 Normalized matrix

	Slp	Ele	Asp.	RB	LULC	STI	SPI	SB	Litho	Soil	LB	∑ rank	[C]	[D]= [A]*[C]	[E]= [D]/[C]	λmax	CI	CR
Slp	0.33	0.41	0.38	0.34	0.30	0.27	0.24	0.22	0.20	0.18	0.17	3.03	0.275	3.368	12.236	11.708	0.071	0.047
Ele	0.17	0.20	0.26	0.26	0.24	0.22	0.20	0.19	0.17	0.16	0.15	2.23	0.202	2.506	12.386			
Asp.	0.11	0.10	0.13	0.17	0.18	0.18	0.17	0.16	0.15	0.14	0.14	1.63	0.149	1.837	12.356			
RB	0.08	0.07	0.06	0.09	0.12	0.13	0.14	0.13	0.13	0.13	0.12	1.20	0.109	1.332	12.173			
LULC	0.07	0.05	0.04	0.04	0.06	0.09	0.10	0.11	0.11	0.11	0.11	0.89	0.080	0.957	11.897			
STI	0.06	0.04	0.03	0.03	0.03	0.04	0.07	0.08	0.09	0.09	0.09	0.65	0.059	0.683	11.594			
SPI	0.05	0.03	0.03	0.02	0.02	0.02	0.03	0.05	0.07	0.07	0.08	0.47	0.043	0.486	11.324			
SB	0.04	0.03	0.02	0.02	0.02	0.01	0.02	0.03	0.04	0.05	0.06	0.34	0.031	0.345	11.143			
Litho	0.04	0.03	0.02	0.01	0.01	0.01	0.01	0.01	0.02	0.04	0.05	0.25	0.022	0.248	11.096			
Soil	0.03	0.02	0.02	0.01	0.01	0.01	0.01	0.01	0.01	0.02	0.03	0.18	0.016	0.183	11.198			
LB	0.03	0.02	0.01	0.01	0.01	0.01	0.01	0.01	0.01	0.01	0.02	0.14	0.012	0.141	11.388			
∑	1.00	1.00	1.00	1.00	1.00	1.00	1.00	1.00	1.00	1.00	1.00	11.00	1.00		128.791			

Table 3 Random index (Saaty 1980)

Number of criteria	2	3	4	5	6	7	8	9	10	11
RI	0.00	0.58	0.90	1.12	1.24	1.32	1.41	1.45	1.49	1.51

where \tilde{r}_i still depicts the triangular values.

Step 5: From the next 3 sub steps (5a, 5b, and 5c), the fuzzy weight of each parameter was computed.

Step 5a: Calculation of vector summation of each \tilde{r}_i

Step 5b: The (-1) power of summation vector was calculated, followed by replacement of the fuzzy triangular number to convert it into an increasing order.

Step 5c: To compute the fuzzy weight of parameters $i(\tilde{w}_i)_i$, each \tilde{r}_i was multiplied with the reverse vector (Eq. 13).

$$\tilde{w}_i = \tilde{r}_i \otimes (\tilde{r}_1 \oplus \tilde{r}_2 \oplus \dots \oplus \tilde{r}_n)^{-1} (lw_i, mw_i, uw_i) \tag{13}$$

Step 6: De-fuzzification of the fuzzy weights using Eq. 14 (Chou and Chang 2008).

$$M_i = \frac{lw_i, mw_i, uw_i}{3} \tag{14}$$

Step 7: The standardization of M_i using Eq. 15.

$$N_i = \frac{M_i}{\sum_{i=1}^n M_i} \tag{15}$$

The final weights obtained using the F-AHP method is shown in Eq. 16.

$$\begin{aligned} \text{LSZ} = & (0.265 \times \text{Slp.}) + (0.208 \times \text{Ele.}) \\ & + (0.155 \times \text{Asp.}) + (0.113 \times \text{RB}) + (0.082 \times \text{LULC}) \\ & + (0.058 \times \text{STI}) + (0.041 \times \text{SPI}) + (0.030 \times \text{SB}) \\ & + (0.021 \times \text{Litho.}) + (0.015 \times \text{Soil}) + (0.011 \times \text{LB}) \end{aligned} \tag{16}$$

Validation using the ROC curve method

The ROC curve method has been used to validate the results. The ROC curve is a plot of test sensitivity as the y coordinate versus its 1-specificity or false positive rate as the x coordinate (Park et al. 2004). AUC is a measure of a test's ability to identify whether a specific condition is present or not (Hoo et al. 2017). To plot the ROC curve and to estimate the AUC values, the RStudio software was used. The AUC value is considered excellent for values between 0.9 and 1.0, good between 0.8 and 0.9, fair between 0.7 and 0.8, poor between 0.6 and 0.7, and failed between 0.5 and 0.6 (Battolla et al. 2017).

Results and discussion

The landslide susceptible zone maps were prepared by considering eleven causative factors, such as slope angle, elevation, aspect, proximity to roads (road buffer), land use/land cover types, STI, SPI, proximity to streams (stream buffer), lithology, soil texture, and proximity to lineaments (lineament buffer). The area of the prepared maps is grouped into five susceptible zones: very low, low, moderate, high, and very high (Tables 8, 9). The prepared maps were validated using the landslide incidence data collected from the records of the GSI. A total of 23 landslides have been recorded in the study area. The major contributing factor is roads, followed by land use/land cover, slope, and SPI. Of the 23 landslides, 16 (69.56%) occurred near the road cuttings. The landslide

Table 4 Pair-wise comparisons of parameters

	Slp	Ele	Asp.	RB	LULC	STI	SPI	SB	Litho	Soil	LB
Slp	(1,1,1)	(1,2,3)	(2,3,4)	(3,4,5)	(4,5,6)	(5,6,7)	(6,7,8)	(7,8,9)	(8,9,10)	(9,10,11)	(11,11,11)
Ele	(1/3,1/2,1)	(1,1,1)	(1,2,3)	(2,3,4)	(3,4,5)	(4,5,6)	(5,6,7)	(6,7,8)	(7,8,9)	(8,9,10)	(9,10,11)
Asp.	(1/4,1/3,1/2)	(1/3,1/2,1)	(1,1,1)	(1,2,3)	(2,3,4)	(3,4,5)	(4,5,6)	(5,6,7)	(6,7,8)	(7,8,9)	(8,9,10)
RB	(1/5,1/4,1/3)	(1/4,1/3,1/2)	(1/3,1/2,1)	(1,1,1)	(1,2,3)	(2,3,4)	(3,4,5)	(4,5,6)	(5,6,7)	(6,7,8)	(7,8,9)
LULC	(1/6,1/5,1/4)	(1/5,1/4,1/3)	(1/4,1/3,1/2)	(1/3,1/2,1)	(1,1,1)	(1,2,3)	(2,3,4)	(3,4,5)	(4,5,6)	(5,6,7)	(6,7,8)
STI	(1/7,1/6,1/5)	(1/6,1/5,1/4)	(1/5,1/4,1/3)	(1/4,1/3,1/2)	(1/3,1/2,1)	(1,1,1)	(1,2,3)	(2,3,4)	(3,4,5)	(4,5,6)	(5,6,7)
SPI	(1/8,1/7,1/6)	(1/7,1/6,1/5)	(1/6,1/5,1/4)	(1/5,1/4,1/3)	(1/4,1/3,1/2)	(1/3,1/2,1)	(1,1,1)	(1,2,3)	(2,3,4)	(3,4,5)	(4,5,6)
SB	(1/9,1/8,1/7)	(1/8,1/7,1/6)	(1/7,1/6,1/5)	(1/6,1/5,1/4)	(1/5,1/4,1/3)	(1/4,1/3,1/2)	(1/3,1/2,1)	(1,1,1)	(1,2,3)	(2,3,4)	(3,4,5)
Litho	(1/10,1/9,1/8)	(1/9,1/8,1/7)	(1/8,1/7,1/6)	(1/7,1/6,1/5)	(1/6,1/5,1/4)	(1/5,1/4,1/3)	(1/4,1/3,1/2)	(1/3,1/2,1)	(1,1,1)	(1,2,3)	(2,3,4)
Soil	(1/11,1/10,1/9)	(1/10,1/9,1/8)	(1/9,1/8,1/7)	(1/8,1/7,1/6)	(1/7,1/6,1/5)	(1/6,1/5,1/4)	(1/5,1/4,1/3)	(1/4,1/3,1/2)	(1/3,1/2,1)	(1,1,1)	(1,2,3)
LB	(1/11,1/11,1/11)	(1/11,1/10,1/9)	(1/10,1/9,1/8)	(1/9,1/8,1/7)	(1/8,1/7,1/6)	(1/7,1/6,1/5)	(1/6,1/5,1/4)	(1/5,1/4,1/3)	(1/4,1/3,1/2)	(1/3,1/2,1)	(1,1,1)

susceptible zone maps are depicted in Figs. 14 and 15. A considerable number of landslides occurred on agricultural land, higher slopes, and in areas with higher SPI. 39.13% and 43.48% of landslide incidences have been recorded in the low susceptible zone of the maps prepared using the

F-AHP and AHP methods, respectively. These landslides have occurred within a 100 m buffer distance of roads. This confirms that the occurrence of landslides in this area is mainly due to anthropogenic reasons (road cuttings). The study found that unscientific hill cutting for road widening

Table 5 Geometric means of fuzzy comparison values

Slp	Fuzzy geometric mean value (\bar{r}_i)		
	3.98	4.91	5.73
Ele	2.90	3.71	4.61
Asp.	2.09	2.72	3.48
RB	1.50	1.96	2.55
LULC	1.07	1.40	1.84
STI	0.76	1.00	1.32
SPI	0.54	0.71	0.94
SB	0.39	0.51	0.67
Litho	0.29	0.37	0.48
Soil	0.22	0.27	0.35
LB	0.17	0.20	0.25
$\sum \bar{r}_i$	13.90	17.77	22.22
$(\sum \bar{r}_i)^{-1}$	0.05	0.06	0.17

Table 6 Relative fuzzy weights of each parameter

Slp	Fuzzy weight (\bar{w}_i)		
	0.179	0.276	1.000
Ele	0.130	0.209	0.804
Asp.	0.094	0.153	0.607
RB	0.067	0.111	0.446
LULC	0.048	0.079	0.322
STI	0.034	0.056	0.230
SPI	0.024	0.040	0.164
SB	0.018	0.029	0.117
Litho	0.013	0.021	0.083
Soil	0.010	0.015	0.060
LB	0.008	0.011	0.044

Table 7 Averaged and normalized relative weights of parameters

	Weight (Mi)	Normalized weight (Ni)
Slp	0.485	0.265
Ele	0.381	0.208
Asp.	0.285	0.155
RB	0.208	0.113
LULC	0.150	0.082
STI	0.107	0.058
SPI	0.076	0.041
SB	0.054	0.030
Litho	0.039	0.021
Soil	0.028	0.015
LB	0.021	0.011
\sum	1.83	1.00

Table 8 Area and percentage of susceptible zones: AHP method

Landslide susceptible zones	Area (Sq. Km)	Percentage of the area of the susceptible zones
Very low	93.71	17.87
Low	153.27	29.23
Moderate	125.54	23.94
High	92.97	17.73
Very high	58.89	11.23
Total	524.38	100

Table 9 Area and percentage of susceptible zones: F-AHP method

Landslide susceptible zones	Area (Sq. Km)	Percentage of the area of the susceptible zones
Very low	91.56	17.46
Low	150.24	28.65
Moderate	127.79	24.37
High	97.27	18.55
Very high	57.52	10.97
Total	524.38	100

and construction and the lack of proper slope protection measures are the major reasons for landslides. Toe erosion is

also one of the main reasons for slope instability. The ROC curve analysis for both the AHP and the F-AHP methods estimated fair AUC values as depicted in Fig. 16.

The hillside roads affect the stability of a slope by overloading and over steepening fill slopes, altering natural flow paths and concentrating water on unstable hill slopes, and undercutting unstable slopes (He et al. 2019). Many researchers (Nepal et al. 2019; Nanda et al. 2020; Pasang and Kubíček 2020; Yin et al. 2020) conducted landslide susceptibility mapping along road cuttings or road corridors. A study by Bui et al. (2012) found road cuttings as one of the major factors influencing landslide occurrence in the Hoa Binh province (Vietnam). He and others (He et al. 2019) in their study conducted in Sichuan, China found that road excavation and rainfall resulted in the

Fig. 14 Landslide susceptible zones: AHP method

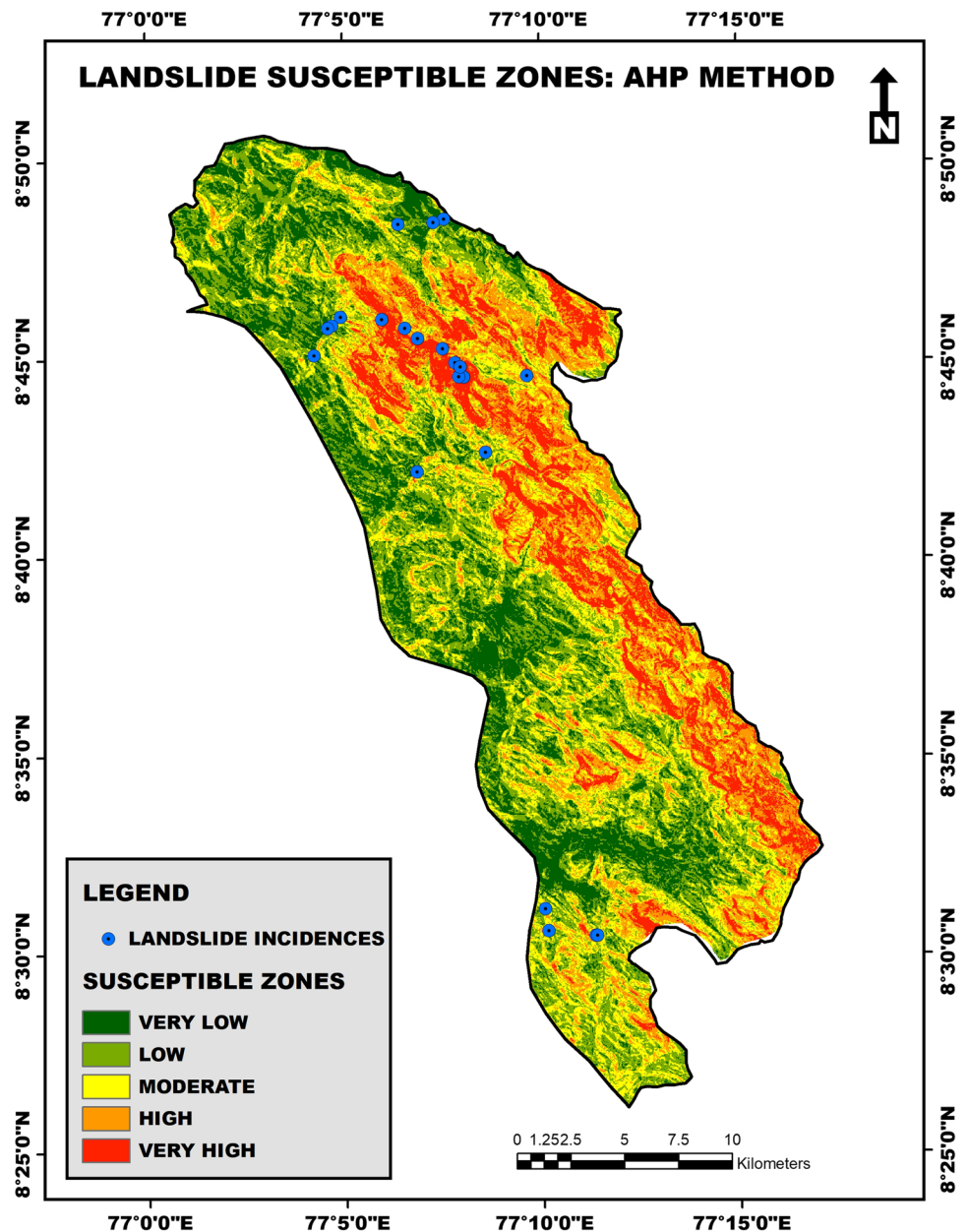
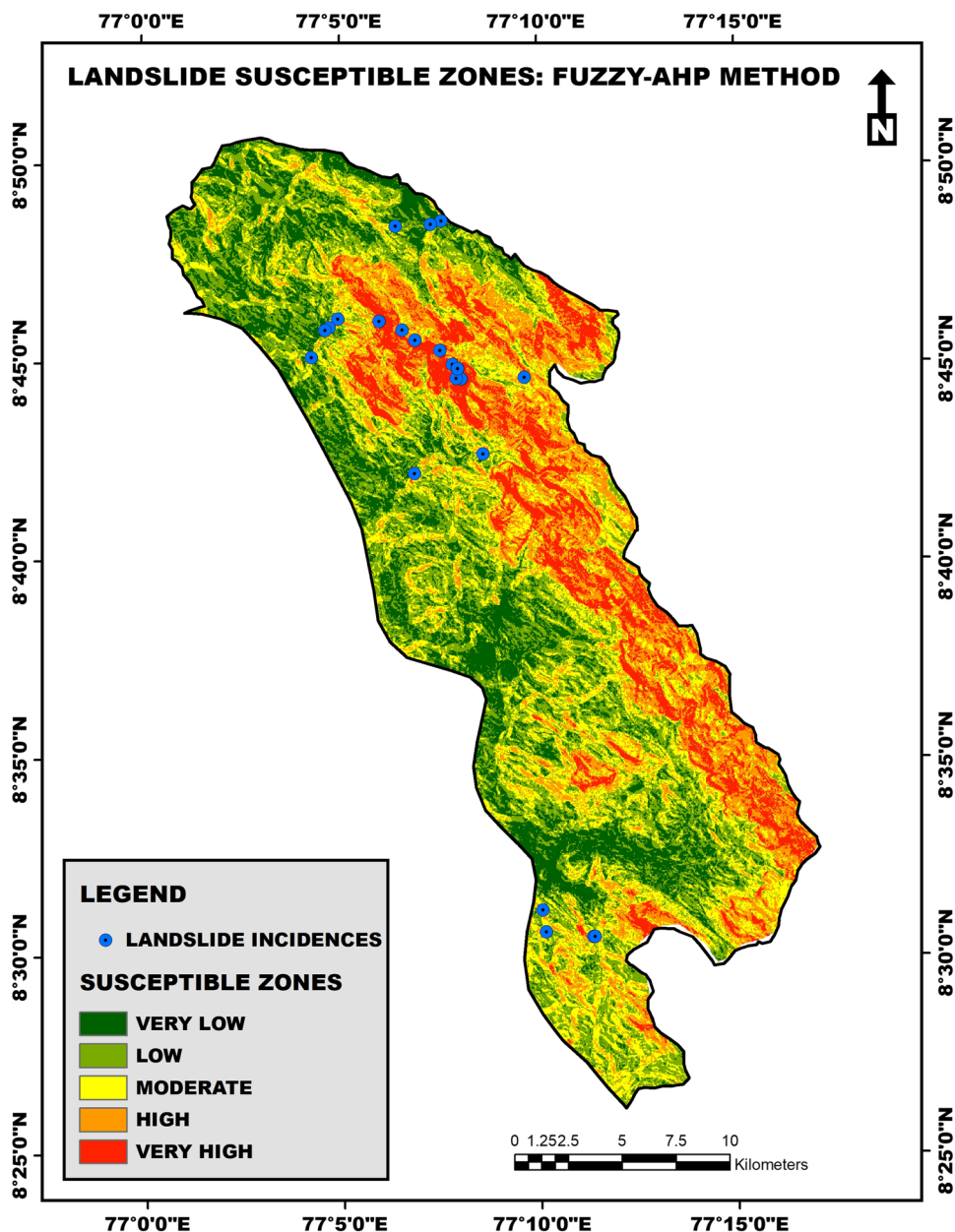


Fig. 15 Landslide susceptible zones: F-AHP method



reactivation of a debris slide. Like the findings of this study, Nanda et al. (2020) also found that human activities like construction of roads and buildings, and agricultural practices are the major reasons for landslide occurrence. Improper land-use practices can decrease the stability of slopes. Karsli et al. (2009) found that the conversion of land cover for agriculture in Ardesen (Turkey) resulted in the occurrence of many landslides with many casualties and property damage. The slope is an important factor influencing landslide occurrence in an area because the downslope shear stress on a particle increases with an increase in slope angle (Rea 2013). In their study, Nakileza and Nedala (2020) found that most of the slope failures were initiated at mid to upper slope positions. Reichenbach et al. (2014) also pointed out the influence of steeper slopes on

soil slide initiation. Getachew and Meten (2021) in their study found that more than 84% of landslides fall on slopes greater than 25°. SPI estimates the capacity of streams to modify the geomorphology of a region through erosion and transportation of materials (Vijith and Dodge-Wan 2019). Poudyal (2012) also found SPI as one of the most influential factors for landslide occurrence.

Conclusions

Due to its unique geological and geomorphological settings, the Western Ghats region is prone to landslides. The landslide susceptible zones in the study area were demarcated

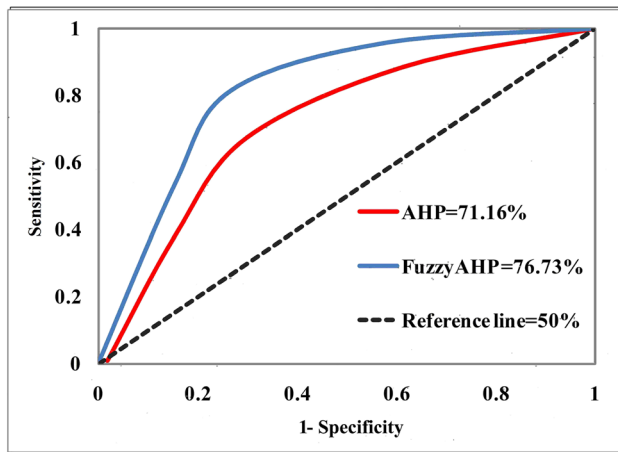


Fig. 16 The ROC curves

using the AHP and F-AHP methods, and the spatial relationship and influence of eleven condition factors were evaluated. The area of the landslide susceptible zones is classified into five zones: very low, low, moderate, high, and very high. The study confirmed road cuttings as the most influential factor. The number of landslides that occurred on agricultural land and close to the streams confirms the influence of agricultural practices and land modifications, and undercutting and erosion by the streams. The validation of the prepared susceptibility maps using the ROC curve method confirmed that both methods can be applied for landslide susceptibility mapping with an AUC value of 0.71 (AHP method), and 0.76 (F-AHP method). As the AUC value for F-AHP is higher, it was selected as the best model. As per the F-AHP model, 10.97% of the study area is classified as a very high landslide susceptible zone. The findings of the study suggest the need for effective mitigation measures, especially nature-based solutions (bioengineering techniques) for landslide mitigation along road cuttings and stream banks, as these are cost effective. The prepared map will be useful for landuse planners and policy makers in adopting suitable measures to reduce the impacts of landslides in areas of similar geoenvironmental conditions.

Funding The authors did not receive any funding from any organization for the submitted work.

Declarations

Conflict of interest The authors have no conflicts of interest to declare.

References

Aditian A, Kubota T, Shinohara Y (2018) Comparison of GIS-based landslide susceptibility models using frequency ratio, logistic

- regression, and artificial neural network in a tertiary region of Ambon, Indonesia. *Geomorphology* 318:101–111. <https://doi.org/10.1016/j.geomorph.2018.06.006>
- Ali SA, Parvin F, Vojteková J, Costache R, Linh NTT, Pham QB, Vojtek M, Gigović L, Ahmad A, Ghorbani MA (2021) GIS-based landslide susceptibility modeling: a comparison between fuzzy multi-criteria and machine learning algorithms. *Geosci Front* 12(2):857–876. <https://doi.org/10.1016/j.gsf.2020.09.004>
- Ayhan MB (2013) A fuzzy AHP approach for supplier selection problem: a case study in a gear motor company. *Int J Manag Value Supply Chains* 4(3):11–23. <https://doi.org/10.5121/ijm-vsc.2013.4302>
- Bachri S, Shrestha RP, Yulianto F, Sumarmi S, Utomo KSB, Aldianto YE (2021) Mapping landform and landslide susceptibility using remote sensing, GIS and field observation in the Southern Cross Road, Malang Regency, East Java, Indonesia. *Geosciences* 11(1):4. <https://doi.org/10.3390/geosciences11010004>
- Bagherzadeh A, Daneshvar MRM (2013) Mapping of landslide hazard zonation using GIS at Golestan watershed, northeast of Iran. *Arab J Geosci* 6:3377–3388. <https://doi.org/10.1007/s12517-012-0583-9>
- Basu T, Pal S (2020) A GIS-based factor clustering and landslide susceptibility analysis using AHP for Gish River Basin, India. *Environ Dev Sustain* 22:4787–4819. <https://doi.org/10.1007/s10668-019-00406-4>
- Battolla E, Canessa PA, Ferro P, Franceschini MC, Fontana V, Dessanti P, Pinelli V, Morabito A, Fedeli F, Pistillo MP, Roncella S (2017) Comparison of the diagnostic performance of fibulin-3 and mesothelin in patients with pleural effusions from malignant mesothelioma. *Anticancer Res* 37(3):1387–1391. <https://doi.org/10.21873/anticancer.11460>
- Buckley JJ (1985) Fuzzy hierarchical analysis. *Fuzzy Sets Syst* 17(1):233–247
- Bui DT, Pradhan B, Lofman O, Revhaug I (2012) Landslide susceptibility assessment in Vietnam using support vector machines, decision tree, and naïve Bayes models. *Math Probl Eng*. <https://doi.org/10.1155/2012/974638>
- Carnero MC (2017) Benchmarking of the maintenance service in health care organizations. In: Noughabi E, Raaheemi B, Albadvi A, Far B (eds) *Handbook of research on data science for effective healthcare practice and administration*. IGI Global, Hershey
- Chauhan S, Sharma M, Arora MK (2010) Landslide susceptibility zonation of the Chamoli region, Garhwal Himalayas, using logistic regression model. *Landslides* 7:411–423. <https://doi.org/10.1007/s10346-010-0202-3>
- Chou SW, Chang YC (2008) The implementation factors that influence the ERP (Enterprise Resource Planning) benefits. *Decis Support Syst* 46(1):149–157
- Constantin M, Bednarik M, Jurchescu MC, Vlaicu M (2011) Landslide susceptibility assessment using the bivariate statistical analysis and the index of entropy in the Sibiciu Basin (Romania). *Environ Earth Sci* 63:397–406. <https://doi.org/10.1007/s12665-010-0724-y>
- Dahal RK, Hasegawa S, Bhandary NP, Poudel PP, Nonomura A, Yatabe R (2012) A replication of landslide hazard mapping at catchment scale. *Geomat Nat Hazards Risk* 3(2):161–192. <https://doi.org/10.1080/19475705.2011.629007>
- Demir G, Aytekin M, Akgün A, İkizler SB, Tatar O (2013) A comparison of landslide susceptibility mapping of the eastern part of the North Anatolian Fault Zone (Turkey) by likelihood-frequency ratio and analytic hierarchy process methods. *Nat Hazards* 65:1481–1506. <https://doi.org/10.1007/s11069-012-0418-8>
- Du W, Wu Y, Liu J, Zhang J, Zhu L (2016) Landslide susceptibility mapping using support vector machine model. *Electron J Geotech Eng* 21:7069–7084
- El Jazouli A, Barakat A, Khellouk R (2019) GIS-multicriteria evaluation using AHP for landslide susceptibility mapping in Oum

- Er Rbia high basin (Morocco). *Geoenviron Disasters* 6:1–12. <https://doi.org/10.1186/s40677-019-0119-7>
- Eskandari S, Miesel JR (2017) Comparison of the fuzzy AHP method, the spatial correlation method, and the Dong model to predict the fire high-risk areas in Hyrcanian forests of Iran. *Geomat Nat Hazards Risk* 8(2):933–949. <https://doi.org/10.1080/19475705.2017.1289249>
- Fatemi Aghda SM, Bagheri V, Razifard M (2018) Landslide susceptibility mapping using fuzzy logic system and its influences on Mainlines in Lashgarak region, Tehran, Iran. *Geotech Geol Eng* 36:915–937. <https://doi.org/10.1007/s10706-017-0365-y>
- Febby B, Achu AL, Jimnisha K, Ayisha VA, Reghunath R (2020) Landslide susceptibility modelling using integrated evidential belief function based logistic regression method: a study from Southern Western Ghats, India. *Remote Sens Appl Soc Environ* 20:100411. <https://doi.org/10.1016/j.rsase.2020.100411>
- Geertsema M, Highland L, Vaugeouis L (2009) Environmental impact of landslides. In: Sassa K, Canuti P (eds) *Landslides: disaster risk reduction*. Springer, Berlin
- Getachew N, Meten M (2021) Weights of evidence modeling for landslide susceptibility mapping of Kabi-Gebro locality, Gunderskel area, Central Ethiopia. *Geoenviron Disasters* 8:1–22. <https://doi.org/10.1186/s40677-021-00177-z>
- Gompf K, Traverso M, Hetterich J (2021) Using analytical hierarchy process (AHP) to introduce weights to social life cycle assessment of mobility services. *Sustainability* 13:1258. <https://doi.org/10.3390/su13031258>
- Harmouzi H, Nefeslioglu HA, Rouai M, Sezer EA, Dekayir A, Gokceoglu C (2019) Landslide susceptibility mapping of the Mediterranean coastal zone of Morocco between Oued Laou and El Jebha using artificial neural networks (ANN). *Arab J Geosci* 12:1–12. <https://doi.org/10.1007/s12517-019-4892-0>
- Hasekiogullari GD, Ercanoglu M (2012) A new approach to use AHP in landslide susceptibility mapping: a case study at Yenice (Karabuk, NW Turkey). *Nat Hazards* 63:1157–1179. <https://doi.org/10.1007/s11069-012-0218-1>
- He K, Ma G, Hu X, Luo G, Mei X, Liu B, He X (2019) Characteristics and mechanisms of coupled road and rainfall-induced landslide in Sichuan China. *Geomat Nat Hazards Risk* 10(1):2313–2329. <https://doi.org/10.1080/19475705.2019.1694230>
- Hoo ZH, Candlish J, Teare D (2017) What is an ROC curve? *Emerg Med J* 34(6):357–359. <https://doi.org/10.1136/emerm-2017-206735>
- Jana SK, Sekac T, Pal DK (2019) Geo-spatial approach with frequency ratio method in landslide susceptibility mapping in the Busu River catchment, Papua New Guinea. *Spat Inf Res* 27:49–62. <https://doi.org/10.1007/s41324-018-0215-x>
- Karsli F, Atasoy M, Yalcin A, Reis S, Demir O, Gokceoglu C (2009) Effects of land-use changes on landslides in a landslide-prone area (Ardesen, Rize, NE Turkey). *Environ Monit Assess* 156:241. <https://doi.org/10.1007/s10661-008-0481-5>
- Kayastha P (2012) Application of fuzzy logic approach for landslide susceptibility mapping in Garuwa sub-basin, East Nepal. *Front Earth Sci* 6:420–432. <https://doi.org/10.1007/s11707-012-0337-8>
- Kayastha P, Bijukchhen SM, Dhital MR, De Smedt F (2013a) GIS based landslide susceptibility mapping using a fuzzy logic approach: a case study from Ghurmi-Dhad Khola area, Eastern Nepal. *J Geol Soc India* 82:249–261. <https://doi.org/10.1007/s12594-013-0147-y>
- Kayastha P, Dhital MR, De Smedt F (2013b) Application of the analytical hierarchy process (AHP) for landslide susceptibility mapping: a case study from the Tinau watershed, west Nepal. *Comput Geosci* 52:398–408. <https://doi.org/10.1016/j.cageo.2012.11.003>
- Kuriakose SL, Sankar G, Muraleedharan C (2009) History of landslide susceptibility and a chorology of landslide-prone areas in the Western Ghats of Kerala, India. *Environ Geol* 57:1553–1568. <https://doi.org/10.1007/s00254-008-1431-9>
- Lee S, Ryu JH, Lee MJ, Won JS (2006) The application of artificial neural networks to landslide susceptibility mapping at Janghung, Korea. *Math Geol* 38:199–220. <https://doi.org/10.1007/s11004-005-9012-x>
- Lee S, Hong SM, Jung HS (2017) A support vector machine for landslide susceptibility mapping in Gangwon Province, Korea. *Sustainability* 9(1):48. <https://doi.org/10.3390/su9010048>
- Mandal S, Mandal K (2018) Modeling and mapping landslide susceptibility zones using GIS based multivariate binary logistic regression (LR) model in the Rorachu river basin of eastern Sikkim Himalaya, India. *Model Earth Syst Environ* 4:69–88. <https://doi.org/10.1007/s40808-018-0426-0>
- Mokarram M, Zarei AR (2018) Landslide susceptibility mapping using Fuzzy-AHP. *Geotech Geol Eng* 36:3931–3943. <https://doi.org/10.1007/s10706-018-0583-y>
- Mondal S, Mandal S (2019) Landslide susceptibility mapping of Darjeeling Himalaya, India using index of entropy (IOE) model. *Appl Geomat* 11:129–146. <https://doi.org/10.1007/s12518-018-0248-9>
- Moore ID, Gessler PE, Nielsen GA, Peterson GA (1993) Soil attribute prediction using terrain analysis. *Soil Sci Soc Am J* 57(2):443–452. <https://doi.org/10.2136/sssaj1993.03615995005700020026x>
- Moore ID, Grayson RB, Ladson AR (1991) Digital terrain modelling: a review of hydrological, geomorphological, and biological applications. *Hydrol Process* 5(1):3–30. <https://doi.org/10.1002/hyp.3360050103>
- NDMA (2019) National landslide risk management strategy, A publication of the National Disaster Management Authority, Government of India, September 2019, New Delhi
- Nachappa TG, Kienberger S, Meena SR, Hölbling D, Blaschke T (2020) Comparison and validation of per-pixel and object-based approaches for landslide susceptibility mapping. *Geomat Nat Hazards Risk* 11(1):572–600. <https://doi.org/10.1080/19475705.2020.1736190>
- Naidu S, Sajinkumar KS, Oommen T, Anuja VJ, Samuel RA, Muraleedharan C (2018) Early warning system for shallow landslides using rainfall threshold and slope stability analysis. *Geosci Front* 9(6):1871–1882. <https://doi.org/10.1016/j.gsf.2017.10.008>
- Nakileza BR, Nedala S (2020) Topographic influence on landslides characteristics and implication for risk management in upper Manafwa catchment, Mt Elgon Uganda. *Geoenviron Disasters* 7:1–13. <https://doi.org/10.1186/s40677-020-00160-0>
- Nanda AM, Hassan ZU, Ahmed P, Kanth TA (2020) Landslide susceptibility assessment of national highway 1D from Sonamarg to Kargil, Jammu and Kashmir, India using frequency ratio method. *GeoJournal*. <https://doi.org/10.1007/s10708-020-10235-y>
- Nepal N, Chen J, Chen H, Wang X, Sharma TPP (2019) Assessment of landslide susceptibility along the Araniko Highway in Poiqu/ Bhote Koshi/Sun Koshi Watershed Nepal, Himalaya. *Prog Disaster Sci* 3:100037. <https://doi.org/10.1016/j.pdisas.2019.100037>
- Nhu VH, Shirzadi A, Shahabi H, Singh SK, Al-Ansari N, Clague JJ, Jaafari A, Chen W, Miraki S, Dou J, Luu C, Gorski K, Pham BT, Nguyen HD, Ahmad BB (2020) Shallow landslide susceptibility mapping: a comparison between logistic model tree, logistic regression, naïve bayes tree, artificial neural network, and support vector machine algorithms. *Int J Environ Res Public Health* 17(8):2749. <https://doi.org/10.3390/ijerph17082749>
- Pal SC, Chowdhuri I (2019) GIS-based spatial prediction of landslide susceptibility using frequency ratio model of Lachung River basin, North Sikkim, India. *SN Appl Sci*. <https://doi.org/10.1007/s42452-019-0422-7>
- Park SH, Goo JM, Jo CH (2004) Receiver operating characteristic (ROC) curve: practical review for radiologists. *Korean J Radiol* 5(1):11–18. <https://doi.org/10.3348/kjr.2004.5.1.11>

- Pasang S, Kubíček P (2020) Landslide susceptibility mapping using statistical methods along the Asian Highway, Bhutan. *Geosciences* 10(11):430. <https://doi.org/10.3390/geosciences10110430>
- Perçin S (2008) Use of fuzzy AHP for evaluating the benefits of information-sharing decisions in a supply chain. *J Enterp Inf Manag* 21(3):263–284. <https://doi.org/10.1108/17410390810866637>
- Pham BT, Pradhan B, Bui DT, Prakash I, Dholakia MB (2016) A comparative study of different machine learning methods for landslide susceptibility assessment: a case study of Uttarakhand area (India). *Environ Modell Softw* 84:240–250. <https://doi.org/10.1016/j.envsoft.2016.07.005>
- Poudyal CP (2012) Landslide susceptibility analysis using decision tree method, Phidim, Eastern Nepal. *Bull Dep Geol* 15:69–76
- Pourghasemi HR, Jirandeh AG, Pradhan B, Xu C, Gokceoglu C (2013) Landslide susceptibility mapping using support vector machine and GIS at the Golestan Province, Iran. *J Earth Syst Sci* 122:349–369. <https://doi.org/10.1007/s12040-013-0282-2>
- Pourghasemi HR, Pradhan B, Gokceoglu C, Moezzi KD (2012) Landslide susceptibility mapping using a spatial multi criteria evaluation model at Haraz Watershed, Iran. In: Pradhan B, Buchroithner M (eds) *Terrigenous mass movements*. Springer, Berlin
- Prasannakumar V, Vijith H (2012) Evaluation and validation of landslide spatial susceptibility in the Western Ghats of Kerala, through GIS-based weights of evidence model and area under curve technique. *J Geol Soc India* 80(4):515–523
- Putra MSD, Andryana S, Fauziah GA (2018) Fuzzy analytical hierarchy process method to determine the quality of gemstones. *Adv Fuzzy Syst*. <https://doi.org/10.1155/2018/9094380>
- Qazi WA (2020) Abushammala MFM (2020) Chapter 10 - Multi-criteria decision analysis of waste-to-energy technologies. In: Ren J (ed) *Waste-to-energy*. Academic Press, Cambridge, pp 265–316
- Rahmati O, Kornejady A, Deo RC (2021) Spatial prediction of landslide susceptibility using random forest algorithm. In: Deo R, Samui P, Kisi O, Yaseen Z (eds) *Intelligent data analytics for decision-support systems in hazard mitigation*. Springer Transactions in Civil and Environmental Engineering. Springer, Singapore
- Ram P, Gupta V, Devi M, Vishwakarma N (2020) Landslide susceptibility mapping using bivariate statistical method for the hilly township of Mussoorie and its surrounding areas, Uttarakhand Himalaya. *J Earth Syst Sci* 129:1–18. <https://doi.org/10.1007/s12040-020-01428-7>
- Ramani SE, Pitchaimani K, Gnanamanickam VR (2011) GIS based landslide susceptibility mapping of Tevankarai Ar sub-watershed, Kodaikkandal, India using binary logistic regression analysis. *J Mt Sci* 8:505–517. <https://doi.org/10.1007/s11629-011-2157-9>
- Rea BR (2013) Permafrost and Periglacial features I blockfields (felsenmeer). In: Elias SA, Mock CJ (eds) *Encyclopedia of quaternary science*, 2nd edn. Elsevier, Amsterdam, pp 523–534
- Reichenbach P, Busca C, Mondini AC, Rossi M (2014) The influence of land use change on landslide susceptibility zonation: the Briga catchment test site (Messina, Italy). *Environ Manag* 54:1372–1384. <https://doi.org/10.1007/s00267-014-0357-0>
- Reis S, Yalcin A, Atasoy M, Nisanci R, Bayrak T, Erduran M, Sancar C, Ekercin S (2012) Remote sensing and GIS-based landslide susceptibility mapping using frequency ratio and analytical hierarchy methods in Rize province (NE Turkey). *Environ Earth Sci* 66:2063–2073. <https://doi.org/10.1007/s12665-011-1432-y>
- Rostami Z, Al-modaresi S, Fathizad H, Faramarzi M (2016) Landslide susceptibility mapping by using fuzzy logic: a case study of Cham-gardalan catchment, Ilam, Iran. *Arab J Geosci* 9:1–11. <https://doi.org/10.1007/s12517-016-2720-3>
- Saaty TL (1980) *The analytic hierarchy process: planning, priority setting, resource allocation* (Decision making series). McGraw Hill, New York
- Sajinkumar KS, Anbazhagan S, Pradeepkumar AP, Rani VR (2011) Weathering and landslide occurrences in parts of Western Ghats, Kerala. *J Geol Soc India*. <https://doi.org/10.1007/s12594-011-0089-1>
- Setiawan I, Mahmud AR, Mansor S, Shariff ARM, Nuruddin AA (2004) GIS-grid-based and multi-criteria analysis for identifying and mapping peat swamp forest fire hazard in Pahang, Malaysia. *Disaster Prev Manag* 13(5):379–386. <https://doi.org/10.1108/09653560410568507>
- Shano L, Raghuvanshi TK, Meten M (2021) Landslide susceptibility mapping using frequency ratio model: the case of Gamo highland, South Ethiopia. *Arab J Geosci* 14:1–18. <https://doi.org/10.1007/s12517-021-06995-7>
- Sharma LP, Patel N, Debnath P, Ghose MK (2012) Assessing landslide vulnerability from soil characteristics: a GIS-based analysis. *Arab J Geosci* 5:789–796. <https://doi.org/10.1007/s12517-010-0272-5>
- Sujatha ER (2020) A spatial model for the assessment of debris flow susceptibility along the Kodaikkandal-Palani traffic corridor. *Front Earth Sci* 14:326–343. <https://doi.org/10.1007/s11707-019-0775-7>
- Sujatha ER, Sridhar V (2017) Mapping debris flow susceptibility using analytical network process in Kodaikkandal Hills, Tamil Nadu (India). *J Earth Syst Sci* 126:1–18. <https://doi.org/10.1007/s12040-017-0899-7>
- Sur U, Singh P, Meena SR (2020) Landslide susceptibility assessment in a lesser Himalayan road corridor (India) applying fuzzy AHP technique and earth-observation data. *Geomat Nat Hazards Risk* 11(1):2176–2209. <https://doi.org/10.1080/19475705.2020.1836038>
- Swetha TV, Gopinath G (2020) Landslides susceptibility assessment by analytical network process: a case study for Kuttiyadi river basin (Western Ghats, southern India). *SN Appl Sci* 2:1–12. <https://doi.org/10.1007/s42452-020-03574-5>
- Taalab K, Cheng T, Zhang Y (2018) Mapping landslide susceptibility and types using Random Forest. *Big Earth Data* 2(2):159–178. <https://doi.org/10.1080/20964471.2018.1472392>
- Talaei R (2014) Landslide susceptibility zonation mapping using logistic regression and its validation in Hashtchin Region, northwest of Iran. *J Geol Soc India* 84:68–86. <https://doi.org/10.1007/s12594-014-0111-5>
- Tsangaratos P, Benardos A (2014) Estimating landslide susceptibility through a artificial neural network classifier. *Nat Hazards* 74:1489–1516. <https://doi.org/10.1007/s11069-014-1245-x>
- Vijith H, Dodge-Wan D (2019) Modelling terrain erosion susceptibility of logged and regenerated forested region in northern Borneo through the analytical hierarchy process (AHP) and GIS techniques. *Geoenviron Disasters* 6:1–18. <https://doi.org/10.1186/s40677-019-0124-x>
- Vijith H, Krishnakumar KN, Pradeep GS, Ninu Krishnan MV, Madhu G (2014) Shallow landslide initiation susceptibility mapping by GIS-based weights-of-evidence analysis of multi-class spatial data-sets: a case study from the natural sloping terrain of Western Ghats, India. *Georisk* 8(1):48–62. <https://doi.org/10.1080/17499518.2013.843437>
- Vijith H, Madhu G (2007) Application of GIS and frequency ratio model in mapping the potential surface failure sites in the Poonjar sub-watershed of Meenachil river in Western Ghats of Kerala. *J Indian Soc Remote Sens* 35:275–285. <https://doi.org/10.1007/BF03013495>
- Wang Y, Song C, Lin Q, Li J (2016) Occurrence probability assessment of earthquake-triggered landslides with Newmark displacement values and logistic regression: the Wenchuan earthquake, China. *Geomorphology* 258:108–119. <https://doi.org/10.1016/j.geomorph.2016.01.004>
- Wu Y, Bai H, Guo Q, Li W (2016) GIS-based landslide susceptibility analysis using support vector machine model at a regional scale. *Electron J Geotech Eng* 21:4427–4434
- Wu Y, Ke Y, Chen Z, Liang S, Zhao H, Hong H (2020) Application of alternating decision tree with AdaBoost and bagging ensembles

- for landslide susceptibility mapping. *CATENA* 187:104396. <https://doi.org/10.1016/j.catena.2019.104396>
- Xiao T, Yin K, Yao T, Liu S (2019) Spatial prediction of landslide susceptibility using GIS-based statistical and machine learning models in Wanzhou County, Three Gorges Reservoir, China. *Acta Geochim* 38:654–669. <https://doi.org/10.1007/s11631-019-00341-1>
- Youssef AM, Pourghasemi HR (2021) Landslide susceptibility mapping using machine learning algorithms and comparison of their performance at Abha Basin, Asir Region, Saudi Arabia. *Geosci Front* 12(2):639–655. <https://doi.org/10.1016/j.gsf.2020.05.010>
- Yin C, Li H, Che F, Li Y, Hu Z, Liu D (2020) Susceptibility mapping and zoning of highway landslide disasters in China. *PLoS ONE* 15(9):e0235780. <https://doi.org/10.1371/journal.pone.0235780>
- Zeng B, Chen X (2021) Assessment of shallow landslide susceptibility using an artificial neural network. *Arab J Geosci*. <https://doi.org/10.1007/s12517-021-06843-8>
- Zhang YX, Lan HX, Li LP, Wu YM, Chen JH, Tian NM (2020) Optimizing the frequency ratio method for landslide susceptibility assessment: a case study of the Caiyuan Basin in the southeast mountainous area of China. *J Mt Sci* 17:340–357. <https://doi.org/10.1007/s11629-019-5702-6>
- Zhou S, Zhou S, Tan X (2020) Nationwide susceptibility mapping of landslides in Kenya using the fuzzy analytic hierarchy process model. *Land* 9(12):535. <https://doi.org/10.3390/land9120535>